UC Irvine
UC Irvine Previously Published Works

Title
Mechanisms of Reactions of Sulfur Hydride Hydroxide: Tautomerism, Condensations, and C–Sulfenylation and O–Sulfenylation of 2,4-Pentanedione

Permalink
https://escholarship.org/uc/item/0zq1p8jw

Journal
The Journal of Physical Chemistry A, 119(14)

ISSN
1089-5639

Author
Freeman, Fillmore

Publication Date
2015-04-09

DOI
10.1021/acs.jpca.5b00779

Copyright Information
This work is made available under the terms of a Creative Commons Attribution License, available at https://creativecommons.org/licenses/by/4.0/

Peer reviewed

eScholarship.org Powered by the California Digital Library
University of California

THE JOURNAL OF PHYSICAL CHEMISTRY A

Article

pubs.acs.org/JPCA

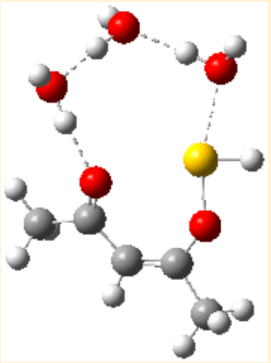
Mechanisms of Reactions of Sulfur Hydride Hydroxide: Tautomerism, Condensations, and C-Sulfenylation and O-Sulfenylation of 2,4-Pentanedione

Fillmore Freeman*

Department of Chemistry, University of California, Irvine, Irvine, California 92697, United States

Supporting Information

ABSTRACT: The conformations, equilibrium structures, hydrogen bonds, and non-covalent interactions involved in the mechanisms of tautomerization, condensations, and C-sulfenylation and O-sulfenylation of 2,4-pentanedione by sulfur hydride hydroxide (hydrogen thioperoxide, oxadisulfane, H−SOH) have been studied using BD(T), CCSD(T), and QCISD(T) with the cc-pVTZ basis set and using B3LYP, B3PW91, CAM-B3LYP, PBE1PBE, PBEh1PBE, LC-ωPBE, M06-2X, and ωB97XD with the 6-311+G(d,p) basis set. All levels of theory predict the sulfenyl (H−SOH) tautomer of hydrogen thioperoxide to be lower in energy than the sulfinyl ($H_2S{=}O$) tautomer. Four reasonable mechanisms were considered for the tautomerization of the sulfenyl tautomer of hydrogen thioperoxide to the sulfinyl tautomer: a cyclic three-membered water-free transition state (**TS**, CCSD(T) activation energy barrier $E^{\ddagger}$ = 65.1 kcal/mol), a cyclic five-membered transition state with one water molecule (**TS**H_2O, $E^{\ddagger}$ = 31.1 kcal/mol), a cyclic seven-membered transition state with two water molecules (**TS**2H_2O, $E^{\ddagger}$ = 14.5 kcal/mol), and a cyclic nine-membered transition state with three water molecules (**TS**3H_2O, $E^{\ddagger}$ = 5.6 kcal/mol). The mechanisms involve hydrogen-bonded reactant complexes and hydrogen-bonded product complexes. The CCSD(T)-predicted energy barriers for the condensation of hydrogen thioperoxide to form thiosulfinic acid through transition states with zero, one, and two waters are $E^{\ddagger}$ = 42.0, 18.3, and 0 kcal/mol, respectively. Mixed condensation reactions are predicted to afford organosulfur products and compounds containing sulfur−selenium bonds. Hydrogen thioperoxide is predicted to add to 2,4-pentanedione to form C-sulfenylated (sulfide, thioether) and O-sulfenylated (sulfenate ester) products. Similar mechanistic trends and reaction pathways are observed in the tautomerism, condensations, and C-sulfenylation and O-sulfenylation reactions of hydrogen thioperoxide. The water molecules set up proton relay networks (bridges) that reduce ring strain, generate favorable conformations for reactivity, lower energy barriers, and increase the numbers of stabilizing hydrogen bonds and nonbonding interactions.



INTRODUCTION

The unstable inorganic compound sulfur hydride hydroxide (hydrogen thioperoxide, oxadisulfane, H−SOH, **1**) (Figure 1) is the simplest oxoacid of sulfur. The **1**-*s*-*cis* and **1**-*s*-*trans* structures in Figure 1 are transition states for the enantiomeric interconversion of **1**. Ultraviolet and laser photolysis of hydrogen sulfide and ozone in an argon matrix afforded **1**.[1,2] The oxidation of hydrogen sulfide by atomic oxygen generated from the photolysis of ozone in an argon matrix was reported to give a mixture of **1** and its sulfinyl tautomer $H_2S{=}O$ (**1a**).[3] Ozone also reacts with hydrogen sulfide to yield **1** and other products.[4−6] Hydrogen thioperoxide has been synthesized in the gas phase by pyrolysis of di-*tert*-butyl sulfoxide (t-$Bu_2S{=}O$).[7,8] Ozone, hydrogen sulfide, and low-molecular-weight compounds of H, S, and O play important roles in atmospheric chemistry and combustion chemistry. Hydrogen thioperoxide may help scientists to understand how similar molecules are formed in the interstellar medium and how pollutants form in the atmosphere of Earth (source of radicals associated with the atmospheric oxidation of sulfides that leads to the production of acid rain and atmospheric haze and to the depletion of ozone).

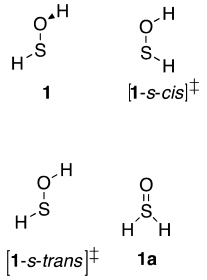


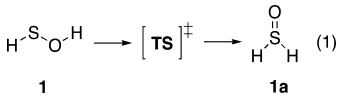
Figure 1. Sulfenyl (**1**) and sulfinyl (**1a**) tautomers of hydrogen thioperoxide.

Although the structural and spectral properties of hydrogen thioperoxide have been extensively studied, relatively little is known about its chemistry. Hydrogen thioperoxide (**1**) and sulfenic acids (R−SOH) exist as sulfenyl (H−SOH, **1**) and sulfinyl ($H_2S{=}O$, C_s, **1a**) tautomers (eq 1).[7−10] Although there are a few

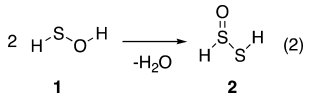
Received: January 25, 2015
Revised: March 10, 2015
Published: March 12, 2015

ACS Publications © 2015 American Chemical Society

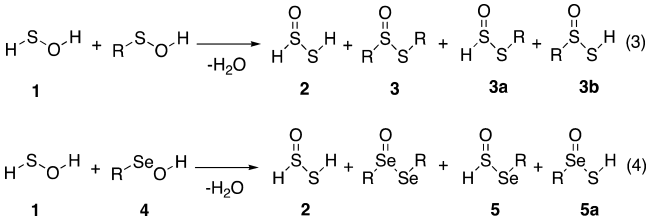
DOI: 10.1021/acs.jpca.5b00779
J. Phys. Chem. A 2015, 119, 3500−3517



exceptions, generally the sulfenyl tautomer is more stable than the corresponding sulfinyl tautomer. Analogous to sulfenic acids, hydrogen thioperoxide is expected to have electrophilic and nucleophilic character, to undergo condensation reactions (cyclodehydration, dehydrative cyclocondensation, self-condensation),[11] and to react with 1,3-dicarbonyl compounds.[12−17] In this study, the mechanisms of the tautomerization of **1** (eq 1), its condensation to form the parent thiosulfinic acid (sulfinothioic acid, **2**) (eq 2),[18,19]



its condensation with other sulfenic acids to form organosulfur compounds (eq 3), its condensation with selenenic acids **4** to



form products **5** containing sulfur−selenium bonds (eq 4),[20−23] and its C-sulfenylation and O-sulfenylation of 2,4-pentanedione (acetylacetone, Figure 2, eq 5) have been investigated in order

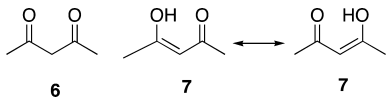
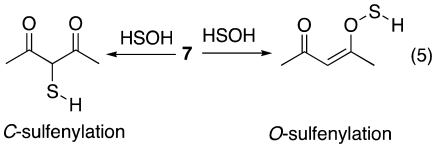


Figure 2. Diketo (**6**) and enolone (**7**) tautomers of 2,4-pentanedione.



to enable a fuller understanding of and deeper insight into the chemistry of the sulfenyl and sulfinyl functional groups in **1** and in sulfenic acids. There are only a few procedures for preparing a diverse range of products with S−Se bonds, and compounds containing S−Se bonds have been implicated in biological processes.[20−23] The mechanisms of C-sulfenylation and O-sulfenylation of 1,3-dicarbonyl compounds are also of importance in the detection of protein sulfenic acids (protein−SOH).[12−17]

2,4-Pentanedione exists as a dynamic equilibrium mixture of tautomers, including the diketo tautomer (**6**) and the dominant enolone tautomer, (3*Z*)-4-hydroxy-3-penten-2-one (ketoenol, **7**) (Figure 2).[24−29] Although the reactions of sulfenic acids with 1,3-dicarbonyl compounds are generally written as resulting in sulfenylation at carbon to form the thioether (sulfide) products, sulfenylation at oxygen to form the sulfenate ester products through the π-conjugated enolone system (eq 5) or through different mechanisms is also reasonable.[12,13] In part because of the transient existence of **1** and sulfenic acids, there is a paucity of fundamental experimental studies of the mechanisms and products of their reactions with chemoselective 1,3-dicarbonyl reagents and with other functional groups. Because of the high reactivity of **1** and sulfenic acids, computational quantum chemistry is an excellent tool to investigate their properties and structures and the mechanisms of their tautomerism, condensation reactions,[11] and C-sulfenylation and O-sulfenylation of 1,3-dicarbonyl compounds.[12−17]

COMPUTATIONAL AND THEORETICAL METHODS

Calculations were carried out with the Gaussian 03[30] and Spartan[31] computational programs. Initial searches for the lowest-energy conformers and rotamers were performed using the MMFF force field and a Monte Carlo algorithm.[31] The lowest-energy conformers and rotamers were reoptimized at several high levels of modern electronic structure theory. Several levels of theory were employed because at some levels different conformers are isoenergetic and the lowest-energy conformer at a given level of theory does not uniformly translate into the lowest-energy conformer at another level. No constraints were imposed on the structures in the equilibrium geometry calculations and transition state structure optimizations.

Equilibrium geometry and frequency calculations were carried out using the density functionals B3LYP,[32] B3PW91,[33−37] PBE1PBE,[33−37] PBEh1PBE,[33−37] M06-2X,[38,39] LC-ωPBE,[40] CAM-B3LYP,[41] and ωX97XD[42] with the triple-ζ 6-311+G(d,p) basis set. Single-point energy calculations were carried out on geometry-optimized low-molecular-weight structures using coupled cluster theory including the singles and doubles with perturbative triples excitations method [CCSD(T)],[43,44] the quadratic configuration interaction singles, doubles, and triples method [QCISD(T)],[45] and the Brueckner doubles method with triples contributions added [BD(T)][46] in conjunction with the correlation-consistent polarized valence cc-pVTZ basis set.[47] The relative energies (ΔE) and activation energy barriers ($E^{\ddagger}$) include the electronic energies plus the zero-point vibrational energies (ZPVEs). The values of $E^{\ddagger}$, ΔE, and thermodynamic parameters[30] were computed relative to the energies of the separated reactants, which were set as the reference at 0.0 kcal/mol. The standard enthalpies and Gibbs free energies of reaction at 298.15 K ($\Delta_r H^\circ$ and $\Delta_r G^\circ$, respectively) were calculated as follows:

$$\Delta_r H^\circ = \sum_{\text{products}} (E_{\text{elec}} + H_{\text{corr}}) - \sum_{\text{reactants}} (E_{\text{elec}} + H_{\text{corr}})$$

$$\Delta_r G^\circ = \sum_{\text{products}} (E_{\text{elec}} + G_{\text{corr}}) - \sum_{\text{reactants}} (E_{\text{elec}} + G_{\text{corr}})$$

Vibrational frequency analyses were also carried out in order to assess the nature of the stationary points and to obtain the ZPVEs. The characteristics of local minima and transition states were verified by establishing that the former did not have an imaginary frequency and that the latter had one imaginary frequency. The vibrational frequencies in the text are not scaled.[48,49] Intrinsic reaction coordinate (IRC) calculations in the forward and reverse directions were used to unambiguously connect transition state structures to their respective reactants, reactant complexes, product complexes, and products.[50] The charge distributions were analyzed using natural population analysis (NPA, natural bond order).[51]

DOI: 10.1021/acs.jpca.5b00779
J. Phys. Chem. A 2015, 119, 3500−3517

Bond angles and dihedral angles (τ) are given in degrees, bond lengths and nonbonded distances in angstroms (Å), total energies in atomic units (au), and values of ΔE, $E^{\ddagger}$, $\Delta_r H°$, and $\Delta_r G°$ in kcal/mol. Entropies are given in entropy units (cal mol^{-1} K^{-1}, eu), atomic charges in electrons, dipole moments (μ) in debyes (D), relative infrared intensities in km mol^{-1}, and vibrational frequencies in wavenumbers (cm^{-1}). In the structures shown in the figures, the values of the bond angles are placed near the second atom in the respective angles.

RESULTS AND DISCUSSION

There has been considerable interest and progress in the development of affordable and reliable quantum-chemical methods for computing accurate structures, dispersion (van der Waals) effects, hydrogen-bonding interactions, and long-distance nonbonding interactions.[52−55] Both diffuse and polarization functions are needed for the determination of accurate structures and relative energies of systems containing multiple hydrogen bonds and multiple nonbonding interactions. New quantum-chemical methods are currently being developed, and it is not always an easy task to select the appropriate levels of theory that will give the most accurate results in terms of barrier heights, hydrogen bonding, non-covalent interactions, structural features, transition state properties, and vibrational frequencies. In order to obtain accurate information concerning the optimum levels of theory for consistently predicting electronic structures, non-covalent interactions, and relative energies, eight density functionals (B3LYP,[32] B3PW91,[33−37] PBE1PBE,[33−37] PBEh1PBE,[33−37] M06-2X,[38,39] LC-ωPBE,[40] CAM-B3LYP,[41] and ωB97XD[42]) were used in this study. It is important to consider a range of modern electronic structure methods in order to compare the computed results and to show the consistency of the predicted trends.

Each model was selected on the basis of its unique computing advantages and strengths. Hybrid density functionals combine accuracy with computational speed and ease of use to give reliable predictions and calculation results. B3LYP is the most widely used density functional, and the meta-hybrid generalized gradient approximation functional M06-2X is known for considering weak non-covalent interactions and for predicting accurate activation barriers. LC-ωPBE is a long-range-corrected functional, CAM-B3LYP is the long-range-corrected version of B3LYP using the Coulomb attenuating method, and ωB97XD includes empirical dispersion and long-range corrections. Although CCSD(T) calculations become computationally more expensive as the size of the system increases, they are known to predict excellent energy results. In this study, BD(T) and QCISD(T) predict relative energy values that are very close to or the same as CCSD(T).

Electronic and Molecular Structures. Strong hydrogen bonds are described very accurately by most standard density functionals. Hydrogen-bonding interactions, electrostatic interactions, and nonbonded interactions at the B3LYP/6-311+G(d,p) level are shown in the figures. Hydrogen-bonding interactions and nonbonding covalent interactions are responsible for conformations and geometries. Directionality, i.e., the donor−proton−acceptor bond angle, which is determined by the direction of the acceptor electron pair, is used to approximate the relative strength of intermolecular hydrogen bonds. The strongest intermolecular hydrogen bonds are those that are close to linear, with O−H···O bond angles near 180°.[56,57]

The nature of bonding in hypervalent molecules has been a topic of considerable discussion.[58−70] The computed S−O bond length is strongly dependent on the level of theory, and density functional theory (DFT) models often calculate longer S−O bond lengths than CCSD(T). CCSD(T)/cc-pCVQZ predicts the S−O and S−H bonds in **1** (cf. Figure 3) to be 1.662 and 1.347 Å, respectively.[7,8] It is generally agreed that the dihedral angle in tautomer **1** (τ = H−S−O−H, anticlinal) is approximately 91°. Several CCSD(T) calculations predict that the short S−O bond (1.4749 Å) in tautomer **1a** weakens the S−H bonds. Although the S−O bonds in sulfoxides and other sulfinyl derivatives are often written as S═O, they have also been described as ylides with highly polarized $S^{+}-O^{-}$ σ bonds.[58,59] The sulfinyl tautomer **1a** of hydrogen thioperoxide is predicted to be a trigonal-pyramidal structure with either a highly polar sulfur−oxygen single bond or a double bond involving d orbitals. The sulfur−oxygen bonds in sulfoxides and sulfones also have been described as double bonds with ionic character.[60] It has also been suggested that the sulfur−oxygen bond is strongly polarized

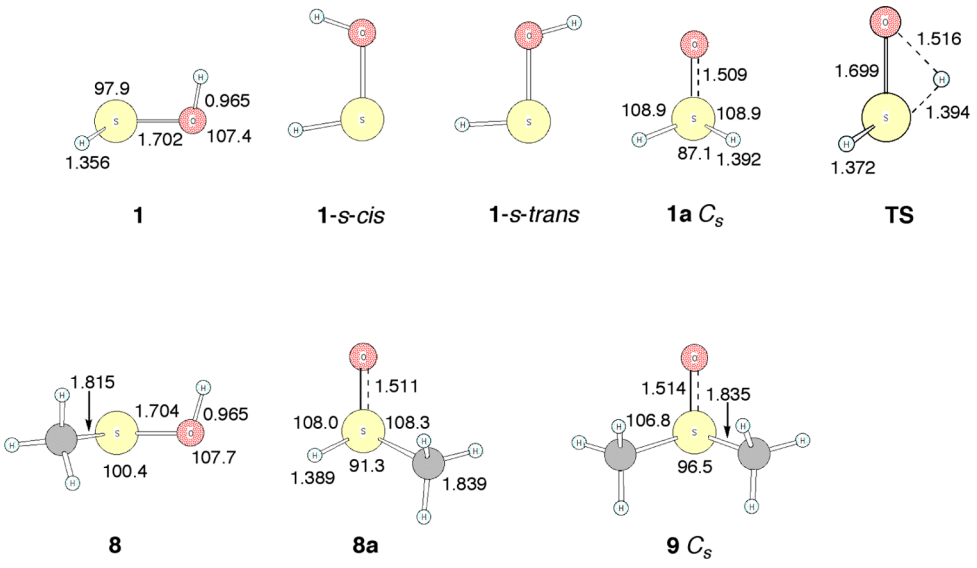


Figure 3. B3LYP-optimized structures of hydrogen thioperoxide tautomers **1** and **1a**, transition states **1**-*s*-*cis*, **1**-*s*-*trans*, and **TS**, methanesulfenic acid tautomers **8** and **8a**, and propanone (**9**).

DOI: 10.1021/acs.jpca.5b00779
J. Phys. Chem. A 2015, 119, 3500−3517

toward oxygen and that the oxygen lone pairs provide pπ−dπ back-bonding to create short, strong S−O bonds.[61] In addition, it has been suggested that d back-bonding does not participate and that the S−O bond is a partially ionic σ bond with partial π bonding through strong n → σ* negative hyperconjugation.[62] The S═O and S−O bond lengths in sulfuric acid are 1.422 and 1.574 Å, respectively. The structures of the transition state for the tautomerism of **1** to **1a** (**TS**), the tautomers of methanesulfenic acid (**8** and **8a**), and propanone (acetone, **9**) are included for comparison in Figure 3. It can be seen in Figure 3 that the sulfur−oxygen bond lengths in **1a**, **8a**, and **9** are similar and that the H−S−H bond angle in **1a** is smaller than the H−S−C angle in **8a** and the C−S−C angle in **9**. The sum of the angles about the sulfur atom in **1a** (304.9°) is smaller than those in **8a** (307.7°) and **9** (310.1°).

Although the conformations of 2,4-pentanedione **6** (Figures 2 and 4) have been extensively studied computationally, experimentally, spectroscopically, and theoretically, there are conflicting reports concerning the ratios, relative energies, and structures of the tautomers due to interpretations of experimental data and to the levels of theory used.[24−29] The C_{2v} structure for enolone 7 has been proposed as either a local minimum or a transition state between the C_s conformers. The C_{2v} conformation of 7 has a symmetrical O···H···O hydrogen bond, whereas an unsymmetrical O−H···O hydrogen bond is predicted for the C_s conformer of 7 (Figure 4). The B3LYP-predicted O···O distance in 7 (Figure 4) is similar to the values reported from electron diffraction (2.592 Å[24] and 2.512 Å[27]) and X-ray crystallography (2.535 Å[28] and 2.547 Å[28]) studies.

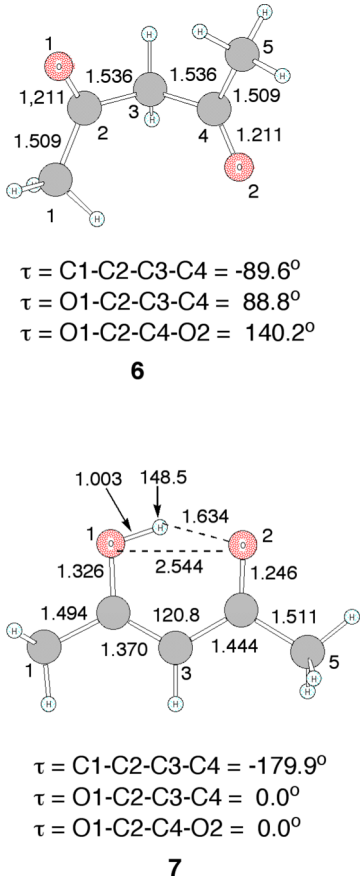


Figure 4. Atom numbering in the B3LYP-optimized diketo (**6**) and enolone (7) tautomers of 2,4-pentanedione.

The tautomeric ratio of **6** and 7 in solution is dependent on the experimental conditions and a variety of different factors including concentration, presence of other species, solvent, and temperature. In agreement with previous reports, all levels of theory used in this study predict that the diketo tautomer **6** and the enolone tautomer 7 are the two lowest-energy tautomers of 2,4-pentanedione (Figure 4) and that 7 is lower in energy than **6** (Table 1). The enolone 7 is stabilized by a strong intramolecular hydrogen bond that results from π delocalization (a resonance-assisted hydrogen bond). The π conjugation in 7 leads to longer C═O bonds and shorter C−C bonds (Figure 4). The O1−H bond in 7 is in the molecular plane, as predicted by the dihedral angle (τ = H−O1−C2−C3) of 0°. Table 1 shows the dependence on and effects of the level of theory in computing the relative energies of the tautomers of hydrogen thioperoxide (**1** and **1a**) and 2,4-pentanedione (**6** and 7). There is better agreement among the density functionals and the single-point energy calculations in predicting the energy difference between tautomers **1** and **1a** than that between tautomers **6** and 7. With a few exceptions, the density functionals predict larger values of the relative energy difference between tautomers **6** and 7 than the three single-point energy calculations BD(T), CCSD(T), and QCISD(T).

Table 1. Relative Energies (ΔE) of the Respective Tautomers of Hydrogen Thioperoxide (1) and 2,4-Pentanedione (6) and Energy Barriers ($E^{\ddagger}$) for the Interconversion of the Enantiomers of 1

	ΔE		$E^{\ddagger}$	
level[a]	**1a**[b]	**6**[c]	**1**-*s*-*cis*[d]	**1**-*s*-*trans*[e]
B3LYP				
$\Delta_r H°$	25.0	5.0	5.6	2.9
$\Delta_r G°$	25.3	4.3	5.8	3.1
$\Delta_r S°$	−1.1	2.2	−0.7	−0.7
B3LYP	25.2	4.7	5.8	3.1
B3PW91	24.2	5.6	6.0	3.2
PBE1PBE	24.6	5.7	6.1	3.2
PBEh1PBE	24.7	5.7	6.1	3.2
M06-2X	29.0	3.6	5.8	3.2
LC-ωPBE	27.5	2.6	6.0	3.3
CAM-B3LYP	27.2	4.6	5.8	3.1
ωB97XD	25.9	2.6	6.0	3.3
BD(T)[f,g]	23.8	4.0	6.4	4.4
CCSD(T)[f,g]	23.8	3.9	6.4	4.4
QCISD(T)[f,g]	23.5	3.8	6.4	4.4

[a]6-311+G(d,p) basis set. [b]$\Delta E = E_{\mathbf{1a}} - E_{\mathbf{1}}$. [c]$\Delta E = E_{\mathbf{6}} - E_{\mathbf{7}}$. [d]$E^{\ddagger} = E_{\mathbf{1}\text{-}s\text{-}cis} - E_{\mathbf{1}}$. [e]$E^{\ddagger} = E_{\mathbf{1}\text{-}s\text{-}trans} - E_{\mathbf{1}}$. [f]cc-pVTZ basis set. [g]B3LYP-optimized structure.

The equilibrium geometries of **1**, **1a**, and the transition states **1**-*s*-*cis* (τ = H−S−O−H = 0°) and **1**-*s*-*trans* (τ = H−S−O−H = 180°) for the interconversion of the enantiomers of **1** are shown in Figure 3. BD(T), CCSD(T), and QCISD(T) predict the energy (rotational) barrier ($E^{\ddagger}$) for the interconversion of **1** via transition state **1**-*s*-*cis* to be 6.4 kcal/mol (Table 1), which is in agreement with the literature reports of 6.2 kcal/mol (aug-cc-PVTZ/MP2)[71−73] and 6.3 kcal/mol (CCSD(T)/cc-pCVQZ).[7,8,72,73] BD(T), CCSD(T), and QCISD(T) predict the energy (rotational) barrier for the interconversion of **1** via **1**-*s*-*trans* to be 4.4 kcal/mol (Table 1),

DOI: 10.1021/acs.jpca.5b00779
J. Phys. Chem. A 2015, 119, 3500−3517

which is in agreement with the reported values of 4.5 kcal/mol (aug-cc-PVTZ/MP2)[71−73] and 4.2 kcal/mol (CCSD(T)/cc-pCVQZ).[7,8,72,73] Similarly, the *s-trans* transition states for the respective interconversions in HOOH and HSSH are also lower in energy than the corresponding *s-cis* transition states.[74]

Tautomerism. The structure of the cyclic three-membered water-free transition state **TS** for the endothermic intramolecular tautomerization of the sulfenyl tautomer of hydrogen thioperoxide **1** to the sulfinyl tautomer **1a** is shown in Figure 3. On the path to transition state **TS**, the sulfur−oxygen bond in **1** becomes shorter, the positive charge on the migrating hydrogen (H_a) on oxygen in **1** (0.471) decreases to 0.321, the negative charge on oxygen (−0.808) increases to −0.860, the positive charge on sulfur increases from 0.250 to 0.453, and the positive charge on the sulfur hydrogen (H_b) remains unchanged at 0.087. The decrease in charge on H_a suggests that electron density is delocalized among the H_a, O, and S atoms in transition state **TS**. The charges on H_a, H_b, S, and O in the ground state of the sulfinyl tautomer **1a** are 0.031, 0.031, 0.851, and −0.914, respectively. CCSD(T) predicts an energy barrier of 64.8 kcal/mol for the tautomerism of **1** to **1a** (Table 2).[8,75,76] It is seen in Table 2 that

Table 2. Energy Barriers and Relative Energies in the Tautomerism of Hydrogen Thioperoxide (1) via Water-Free Transition State TS and via Water-Assisted Transition State TSH_2O

	via **TS**[b]	via TSH_2O[c]			
level[a]	$E_1^{\ddagger}$ [d]	ΔE_1 [e]	$E_2^{\ddagger}$ [f]	ΔE_2 [g]	ΔE_3 [h]
B3LYP	61.8	−5.1	31.3	−6.4	18.8
B3PW91	61.0	−4.7	29.1	−5.6	18.5
PBE1PBE	61.8	−5.9	27.8	−7.2	17.4
PBEh1PBE	61.8	−6.0	27.9	−7.3	17.3
M06-2X	66.4	−6.4	32.2	−8.7	20.3
LC-ωPBE	65.9	−5.4	32.1	−7.3	20.1
CAM-B3LYP	65.0	−6.2	31.4	−8.1	19.1
ωB97XD	64.2	−6.1	32.1	−7.4	18.5
BD(T)[i,j]	65.8	−7.8	31.4	−9.0	14.9
CCSD(T)[i,j]	64.8	−7.8	31.1	−8.9	14.8
QCISD(T)[i,j]	65.1	−7.8	31.1	−8.9	14.6

[a]6-311+G(d,p) basis set. [b]See Figure 3 for the structures. [c]See Figure 5 for the structures. [d]$E_1^{\ddagger} = E_{TS} - E_1$. [e]$\Delta E_1 = E_{\mathbf{1}\cdots H_2O\ \text{reactant complex}} - (E_1 + E_{H_2O})$. [f]$E_2^{\ddagger} = E_{TSH_2O} - (E_1 + E_{H_2O})$. [g]$\Delta E_2 = E_{\mathbf{1a}\cdots H_2O\ \text{product complex}} - (E_{1a} + E_{H_2O})$. [h]$\Delta E_3 = E_{\mathbf{1a}\cdots H_2O\ \text{product complex}} - (E_1 + E_{H_2O})$. [i]cc-pVTZ basis set. [j]B3LYP-optimized structure.

B3LYP, B3PW91, PBE1PBE, and PBEh1PBE predict a lower energy barrier for the tautomerism of **1** to **1a** than the other models.

The CCSD(T)-predicted large energy barrier for the tautomerism of **1** through water-free transition state **TS** suggests that other pathways may be more probable. Tautomers of hydrogen thioperoxide **1** and sulfenic acids form hydrogen-bonded complexes with water, and it is known that the participation of water molecules in transition state structures can lower energy barriers.[12−14,77,78] In view of the ability of water to mediate the long-range transfer of a proton via hydrogen-bonded networks (bridges), tautomerism mechanisms incorporating one, two, or three explicit water molecules were also investigated. The first step in each mechanism involving explicit water molecules is the formation of the reactant complex. Figure 5 shows the reactant complexes, transition states, and product complexes predicted for the mechanisms involving the participation of one, two, and three water molecules in the tautomerization of hydrogen thioperoxide **1** (eq 1).

Incorporating one water molecule into the tautomerism mechanism (**TS**H_2O) lowers the energy barrier $E^{\ddagger}$ from 64.8 to 31.1 kcal/mol (Figures 5 and 6 and Table 2). It can be seen in Figures 5 and 6 that **1** forms a hydrogen-bonded reactant complex that is lower in energy than the separated reactants. The reactant complex rearranges to a cyclic five-membered water-assisted transition state **TS**H_2O that leads to a cyclic five-membered product complex that is higher in energy than the separated reactants and lower in energy than the separated products. A comparison of the sulfur···H−OH distances in the reactant complexes in Figure 5 shows that increasing the number of water molecules brings the migrating hydrogen that is being relayed via the water molecule(s) closer to the migration terminus at sulfur. It can also be seen in Figure 5 that the structures containing three water molecules have the strongest hydrogen bonds.

It can be seen in Table 3 that the inclusion of two water molecules into the mechanism (**TS**$2H_2O$) lowers the energy barrier from 31.1 to 14.5 kcal/mol, whereas the incorporation of three water molecules in the mechanism (**TS**$3H_2O$) lowers the energy barrier to 5.6 kcal/mol and predicts the product complex to be lower in energy than the separated reactants and separated products. In the mechanisms involving water molecules, the reactant complexes and product complexes are better stabilized than the respective separated reactants and separated products. A comparison of the data in Tables 2 and 3 shows that increasing the number of water molecules increases the energy difference between the reactant complex and the separated reactants, increases the energy difference between the product complex and the separated products, and lower the energy difference between the product complex and the separated reactants. Table 3 shows that the energy of the **1a**---$2H_2O$ product complex is closer to the energy of the separated reactants whereas the **1a**---$3H_2O$ product complex is lower in energy that the separated reactants. Water molecules lower the activation energy barrier for tautomerization but do not change the relative energy difference between the respective tautomers.

Increasing the number of water molecules in the mechanism increases the number of hydrogen-bonding interactions that contribute to the stabilization of the structures. There are stronger hydrogen bonds in the three-water structures than in the one-water and two-water structures (Figure 5). The entropic effects were estimated at the B3LYP/6-311+G(d,p) level relative to the sum of the entropies of the separated reactants as a reference point (0 eu). The entropy difference between **1** and transition state **TS** is less than 1 eu. The inclusion of one, two, and three water molecules in the water bridges in the transition state structures increases the entropy by 45.1 eu per each additional water molecule. These estimates may be high because this approach neglects the hydrogen bonding in the reactants (cf. the reactant complexes). The incorporation of explicit water molecules helps to relieve strain, stabilize charges, form conformations that are favorable for reactivity, and set up proton relay networks to facilitate proton transfer from the oxygen in **1** to sulfur in tautomer **1a** via water molecules in a Grotthuss-type mechanism.[12−14,78−84] In the transition state structures, the water molecules act as both proton acceptors and proton donors.

Condensation. Two molecules of **1** interact to form a hydrogen-bonded reactant complex **1**---**1** that is lower in energy than the separated reactants (Figure 7 and Table 4). It can be seen that there is excellent agreement among the levels of theory

DOI: 10.1021/acs.jpca.5b00779
J. Phys. Chem. A 2015, 119, 3500−3517

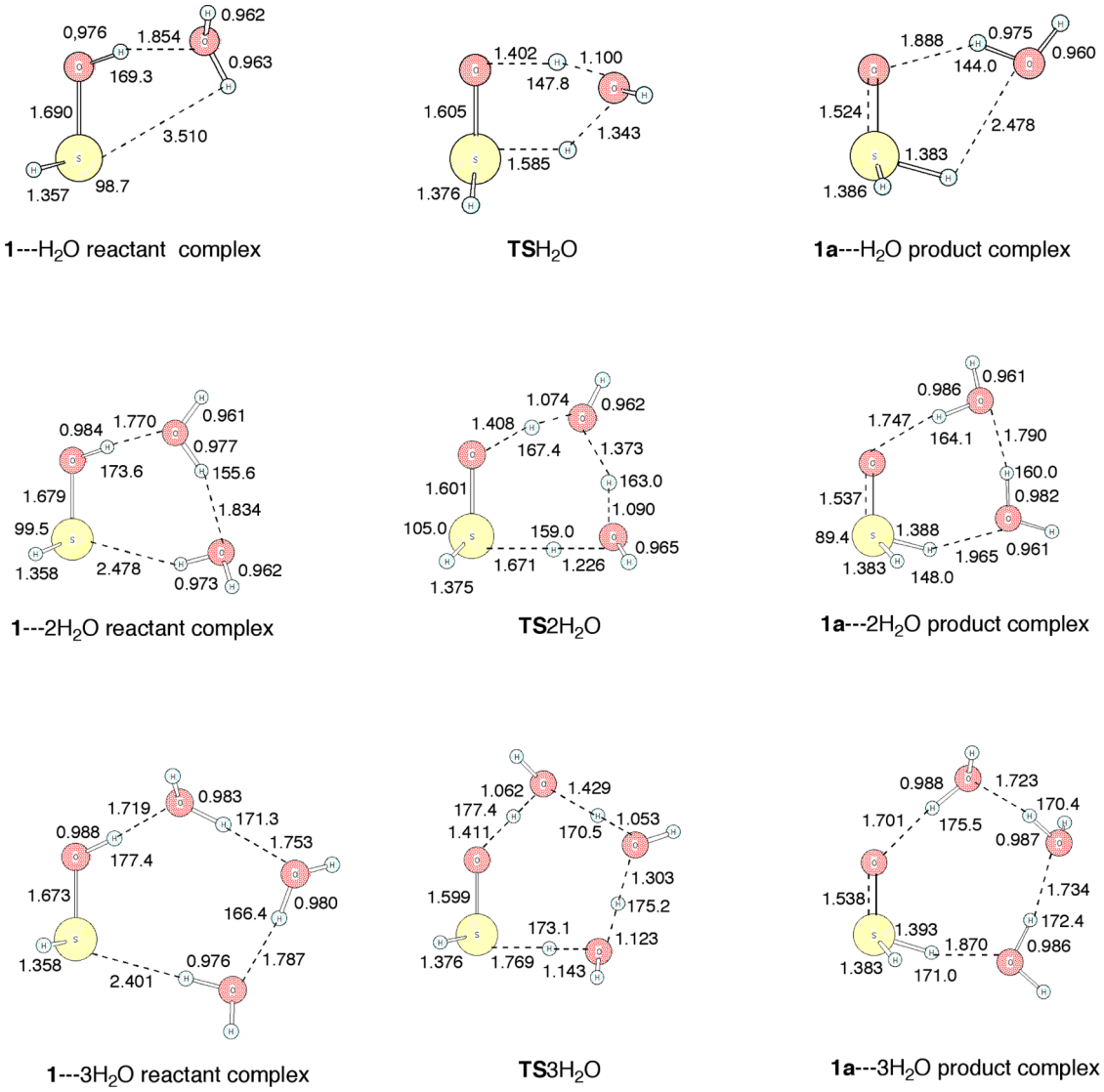


Figure 5. B3LYP-optimized structures of the reactant complexes, transition states, and product complexes for the tautomerism of hydrogen thioperoxide (**1**) with (top) one, (middle) two, and (bottom) three explicit water molecules.

in predicting the energy difference between the reactants **1** and the reactant complex. The **1**---**1** reactant complex rearranges to a cyclic five-membered transition state structure **TS1** that leads to the cyclic **2**---H_2O product complex, which is lower in energy than the separated reactants and lower in energy than the separated products. Figure 7 shows the electrostatic interactions between oxygen and sulfur and between oxygen and the sulfinyl hydrogen in these structures. CCSD(T) predicts the energy barrier for condensation in the absence of water to be $E^{\ddagger}$ = 42.0 kcal/mol (Table 4). M06-2X, CAM-B3LYP, and ωB97XD predict an energy barrier close to that of BD(T), CCSD(T), and QCISD(T), whereas B3LYP, B3PW91, PBE1PBE, and PBEh1PBE predict a lower energy barrier than the other functionals. The sulfur−oxygen bond in the product, sulfinothioic acid (**2**), is shorter than those in **1a**, **8a**, and **9** (Figure 3) and in the **2**---H_2O product complex, which suggests there is more double-bond character in the sulfur−oxygen bond in **2** than in **1a**, **8a**, **9**, and the **2**---H_2O product complex.

Incorporation of a water molecule into the mechanism for the condensation of **1** to **2** (**TS1**H_2O) lowers the CCSD(T)-predicted energy barrier $E^{\ddagger}$ from 42.0 to 18.3 kcal/mol (Table 4 and Figure 7). Figure 8 and Table SI 1 in the Supporting Information (SI) show that incorporation of two water molecules into the mechanism (**TS1**$2H_2O$) lowers the energy barrier to ∼0 kcal/mol. The addition of the second water molecule removes the energy barrier and catalyzes the condensation reaction.[77] At the B3LYP/6-311+G(d,p) level, the entropy of transition state **TS1** is approximately 38.3 eu lower than that of the reactants (two molecules of **1**), and the inclusion of one and two water molecules in the water bridges in the transition state structures decreases the entropy by 45.1 eu per water molecule. The decrease in entropy is consistent with a cycloaddition reaction mechanism. As seen in the tautomerism mechanisms above, the condensation mechanisms with water molecules involve reactant complexes and product complexes that are better stabilized than the respective separated reactants and separated products. A comparison of the data in Table 4 and Table SI 1 shows that increasing the number of water molecules increases the energy differences between the reactant complexes and the separated reactants, between the product complexes and the separated reactants, and between the product complexes and the separated products.[12−14,78−84]

DOI: 10.1021/acs.jpca.5b00779
J. Phys. Chem. A 2015, 119, 3500−3517

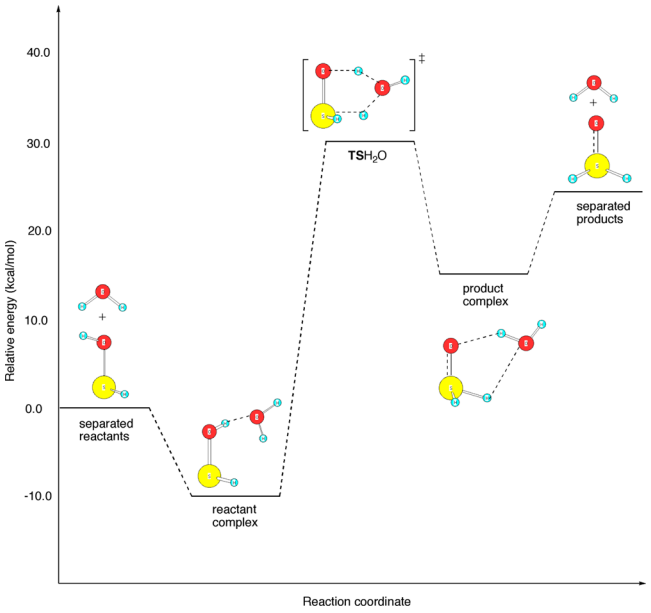


Figure 6. Reaction coordinate for the tautomerization of hydrogen thioperoxide (**1**) with one explicit water molecule.

The cyclic water-free transition state **TS1** is more strained than the transition states containing water molecules. In addition, stronger hydrogen bonds are observed in the transition state structures containing water molecules, and strong hydrogen bonds also help to stabilize the water-containing product complexes (Figure 7). In the water-free **1**---**1** reactant complex (Figure 7) the sulfur atoms are far apart, whereas in the **1**---**1**---H_2O reactant complex the water molecule is strongly hydrogen-bonded to two molecules of **1** in a conformation that brings the two sulfur atoms closer together to form transition state **TS1**H_2O for cyclocondensation. Figure 7 shows that the **1**---**1**---$2H_2O$ reactant complex is in a favorable conformation to initiate partial S···S bond formation in transition state **TS1**$2H_2O$.

Sulfur hydride hydroxide **1** is predicted to undergo condensation with selenium hydride hydroxide (**10**) to afford the isomeric products selenothiosulfinate (**11**) and thioseleninate (**11a**) (Figure 9). BD(T), CCSD(T), and QCISD(T) predict **11** to be 5.3, 5.3, and 5.1 kcal/mol, respectively, lower in energy than **11a**. Similarly, **1** is predicted to undergo condensation with methanesulfenic acid (**8**) to give methanesulfinothioic acid (**12**)[18,19] and hydro(methanethiolato)oxosulfur (**12a**) (eq 3, Figure 10). BD(T), CCSD(T), and QCISD(T) predict **12** to be 5.3 kcal/mol lower in energy than **12a**. The trends observed for the condensation of **1** through water-free transition state **TS1** are also observed for the condensations of **1** with **10** and **8** through water-free transition states **TS2** and **TS3**, respectively (Tables SI 2 and SI 3 in the Supporting Information). Examples of condensations of different sulfenic acids to form isomeric thiosulfinates are found in the chemistry of garlic and onion.[85,86]

C-Sulfenylation and O-Sulfenylation. Hydrogen thioperoxide **1** interacts with enolone **7** to give the *C*-**1**---**7** reactant complex, which lies lower in energy than the isolated reactants and rearranges to the cyclic nearly symmetrical hydrogen-bonded transition state structure **TS4** (C_s-symmetric; Figure 11). It can be seen that in transition state **TS4** the carbonyl groups adopt a cis geometry involving the nascent water molecule bridge that has a hydrogen bond with O2. There is a favorable electrostatic interaction between O2 and S in **TS4** that also contributes to its stabilization. The respective O1−H and H−O3 distances in **TS4** suggest that the proton has been extensively transferred from O1 to O3 of the sulfenyl group of **1**. The breaking of the O1−H bond starts the nucleophilic attack of C3 in **7** at the electrophilic sulfur of hydrogen thioperoxide **1**. Simultaneously, the C2−O1 distance becomes shorter as the carbonyl group forms and the C2−C3 bond distance becomes longer as the hybridization of C3 changes from sp^2 to sp^3. At the same time, the O1 proton interacts with O3 of the sulfenyl group in **1** to convert OH into the better leaving group water. As the O1 proton−O3 bond and the C3−S bond are forming, the S−O3 bond is breaking. The point group, the same negative NPA charges on C1 and C5, the equal C2−O1 and C4−O2 bond distances, and the shorter C2−C3 and C3−C4 bond distances in **TS4** are consistent with π-electron delocalization in the conjugated system (cf. Figures 4 and 11). **TS4** affords the **13**---H_2O product complex, whose energy is lower than that of the separated

Table 3. Energy Barriers and Relative Energies in the Tautomerism of 1 via Water-Assisted Transition States TS2H_2O and TS3H_2O

	via TS2H_2O[b]				via TS3H_2O[b]			
level[a]	ΔE_1[c]	$E_1^{\ddagger}$[d]	ΔE_2[e]	ΔE_3[f]	ΔE_4[g]	$E_2^{\ddagger}$[h]	ΔE_5[i]	ΔE_6[j]
B3LYP	−12.4	14.9	−16.3	8.9	−20.1	6.1	−24.8	0.3
B3PW91	−11.5	13.2	−14.9	9.2	−18.6	4.8	−23.0	1.1
PBE1PBE	−14.4	10.4	−18.1	6.6	−22.8	0.5	−27.5	−2.9
PBEh1PBE	−14.7	10.3	−18.4	6.2	−23.2	0.4	−28.0	−3.3
M06-2X	−14.8	13.7	−19.6	9.4	−22.8	3.9	−28.0	1.0
LC-ωPBE	−12.4	15.7	−17.3	10.1	−20.1	6.9	−25.9	1.5
CAM-B3LYP	−14.6	13.3	−19.4	7.8	−23.4	3.1	−29.2	−2.0
ωB97XD	−14.3	14.6	−18.6	7.3	−22.7	5.3	−27.7	−1.8
BD(T)[k,l]	−19.0	14.5	−20.8	3.1	−28.7	5.5	−30.9	−7.0
CCSD(T)[k,l]	−19.0	14.5	−20.7	3.0	−28.7	5.6	−30.8	−7.0
QCISD(T)[k,l]	−19.1	14.3	−20.7	2.8	−28.8	5.3	−30.8	−7.3

[a] 6-311+G(d,p) basis set. [b] See Figure 5 for the structures. [c] $\Delta E_1 = E_{\mathbf{1}\text{---}2H_2O\ \text{reactant complex}} - (E_{\mathbf{1}} + 2E_{H_2O})$. [d] $E_1^{\ddagger} = E_{TS2H_2O} - (E_{\mathbf{1}} + E_{2H_2O})$. [e] $\Delta E_2 = E_{\mathbf{1a}\text{---}2H_2O\ \text{product complex}} - (E_{\mathbf{1a}} + 2E_{H_2O})$. [f] $\Delta E_3 = E_{\mathbf{1a}\text{---}2H_2O\ \text{product complex}} - (E_{\mathbf{1}} + 2E_{H_2O})$. [g] $\Delta E_4 = E_{\mathbf{1}\text{---}3H_2O\ \text{reactant complex}} - (E_{\mathbf{1}} + 3E_{H_2O})$. [h] $E_2^{\ddagger} = E_{TS3H_2O} - (E_{\mathbf{1}} + 3E_{H_2O})$. [i] $\Delta E_5 = E_{\mathbf{1a}\text{---}3H_2O\ \text{product complex}} - (E_{\mathbf{1a}} + 3E_{H_2O})$. [j] $\Delta E_6 = E_{\mathbf{1a}\text{---}3H_2O\ \text{product complex}} - (E_{\mathbf{1}} + 3E_{H_2O})$. [k] cc-pVTZ basis set. [l] B3LYP-optimized structure.

DOI: 10.1021/acs.jpca.5b00779
J. Phys. Chem. A 2015, 119, 3500−3517

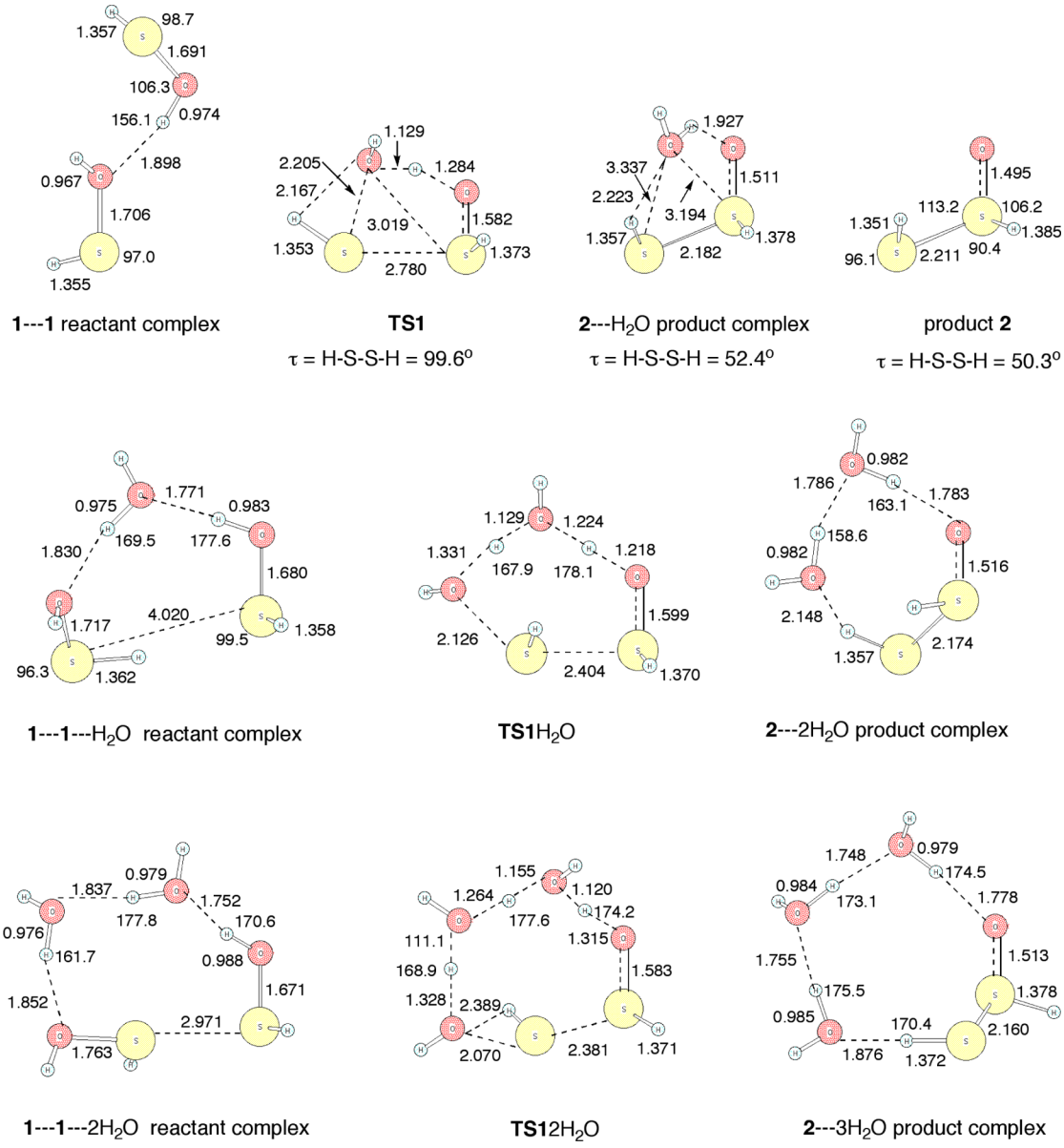


Figure 7. Dihedral angles (τ), electrostatic interactions, and hydrogen bonds in the B3LYP-optimized structures of the reactant complexes, transition states, product complexes, and product **2** in the condensations of hydrogen thioperoxide **1** assisted by (top) zero, (middle) one, and (bottom) two water molecules.

reactants **1** and **7** and close to the sum of the energies of the thioether (sulfide) product, 3-mercapto-2,4-pentanedione (**13**), and one water molecule (Table 5). Two conformations (**13a** and **13aa**) of (3*Z*)-4-hydroxy-3-mercapto-3-penten-2-one, the tautomer of product **13**, are also shown in Figure 11. IRC calculations unambiguously connect **TS4** to the *C*-**1**---**7** reactant complex and the **13**---H_2O product complex.

On going from reactants **1** + **7** through the *C*-**1**---**7** reactant complex to **TS4**, the positive charge at C2 in **7** has increased from 0.462 to 0.510, the negative charge at C3 has decreased from −0.463 to −0.459, and the positive charge at C4 has decreased from 0.525 to 0.510 (Table SI-4 in the Supporting Information). It can also be seen in Table SI-4 that the positive charge at S in **1** has decreased from 0.250 to 0.139 and the positive charge on the sulfanyl hydrogen (S−H) has increased from 0.087 to 0.102 in **TS4**, while the negative charge at O3 in **1** has decreased from −0.808 to −0.774 in **TS4**. The C3−S−O3 bond angle in **TS4** is 71.7°. The transition state structure **TS4** is similar to those predicted for the C-sulfenylation of 5,5-dimethyl-1,3-cyclohexanedione (dimedone) by cysteine sulfenic acid (Cys−SOH)[13] and the C-sulfenylation of 1,3-cyclohexanedione by methanesulfenic acid (**8**).[14]

Enolones are neutral soft nucleophiles that favor conjugate attack. Conjugate addition involving exchange of the nucleophilic centers C3 and O2 in **7** could lead to O-sulfenylation at O2. Although other plausible mechanisms are possible, a reasonable mechanism for the O-sulfenylation of enolone **7** by hydrogen thioperoxide **1** may be similar to that for C-sulfenylation and involve conjugate addition of **1** to O2 in **7** (Figures 11 and 12).[12,13] Figure 12 shows that the O-sulfenylation of **7** by **1** involves a structurally different reactant complex than that predicted for C-sulfenylation (cf. Figures 11 and 12). The interaction of **1** and enolone **7** gives the *O*-**1**---**7** reactant complex, which lies lower in energy than the separated reactants (Table 5) and rearranges to the cyclic transition state structure **TS5** (Figure 12). IRC calculations unambiguously

DOI: 10.1021/acs.jpca.5b00779
J. Phys. Chem. A 2015, 119, 3500−3517

Table 4. Energy Barriers and Relative Energies in the Condensation of Hydrogen Thioperoxide (1) via Water-Free Transition State TS1 and via Water-Assisted Transition State TS1H_2O

	via TS1[b]					via TS1H_2O[b]				
level[a]	ΔE_1[c]	$E_1^{\ddagger}$[d]	ΔE_2[e]	ΔE_3[f]	ΔE_4[g]	ΔE_5[h]	$E_2^{\ddagger}$[i]	ΔE_6[j]	ΔE_7[k]	ΔE_8[l]
B3LYP	−5.1	34.4	−7.1	−15.8	−9.9	−11.8	14.6	−15.3	−25.2	−9.9
B3PW91	−4.5	34.4	−6.6	−17.1	−11.9	−10.7	13.1	−13.9	−25.9	−11.9
PBE1PBE	−5.9	34.5	−8.6	−19.0	−11.8	−13.8	10.2	−17.6	−29.4	−11.8
PBEh1PBE	−6.0	34.3	−8.8	−19.0	−11.6	−14.0	10.0	−18.1	−29.6	−11.6
M06-2X	−6.7	41.4	−10.6	−15.4	−5.4	−14.8	13.7	−20.8	−26.2	−5.4
LC-ωPBE	−5.3	47.2	−8.7	−13.4	−5.6	−12.1	20.7	−17.5	−23.1	−5.6
CAM-B3LYP	−6.1	41.1	−9.3	−14.0	−5.8	−14.0	16.3	−19.2	−25.0	−5.8
ωB97XD	−6.0	41.1	−8.9	−16.7	−8.7	−14.1	17.4	−18.8	−27.5	−8.7
BD(T)[m,n]	−6.7	42.7	−10.7	−19.9	−10.6	−16.4	18.3	−21.1	−31.6	−10.6
CCSD(T)[m,n]	−6.7	42.0	−10.7	−19.9	−10.6	−16.4	18.3	−21.0	−31.6	−10.6
QCISD(T)[m,n]	−6.7	40.8	−10.7	−20.3	−11.0	−16.4	17.8	−21.0	−32.0	−11.0

[a] 6-311+G(d,p) basis set. [b] See Figure 7 for the structures. [c] $\Delta E_1 = E_{\mathbf{1}\text{---}1 \text{ reactant complex}} - 2E_{\mathbf{1}}$. [d] $E_1^{\ddagger} = E_{\mathbf{TS1}} - 2E_{\mathbf{1}}$. [e] $\Delta E_2 = E_{\mathbf{2}\text{---}H_2O \text{ product complex}} - (E_{\mathbf{2}} + E_{H_2O})$. [f] $\Delta E_3 = E_{\mathbf{2}\text{---}H_2O \text{ product complex}} - 2E_{\mathbf{1}}$. [g] $\Delta E_4 = (E_{\mathbf{2}} + E_{H_2O}) - 2E_{\mathbf{1}}$. [h] $\Delta E_5 = E_{\mathbf{1}\text{---}\mathbf{1}\text{---}H_2O \text{ reactant complex}} - (2E_{\mathbf{1}} + E_{H_2O})$. [i] $E_2^{\ddagger} = E_{\mathbf{TS1}H_2O} - (2E_{\mathbf{1}} + E_{H_2O})$. [j] $\Delta E_6 = E_{\mathbf{2}\text{---}2H_2O \text{ product complex}} - (E_{\mathbf{2}} + 2E_{H_2O})$. [k] $\Delta E_7 = E_{\mathbf{2}\text{---}2H_2O \text{ product complex}} - (2E_{\mathbf{1}} + E_{H_2O})$. [l] $\Delta E_8 = (E_{\mathbf{2}} + 2E_{H_2O}) - (2E_{\mathbf{1}} + E_{H_2O})$. [m] cc-pVTZ basis set. [n] B3LYP-optimized structure.

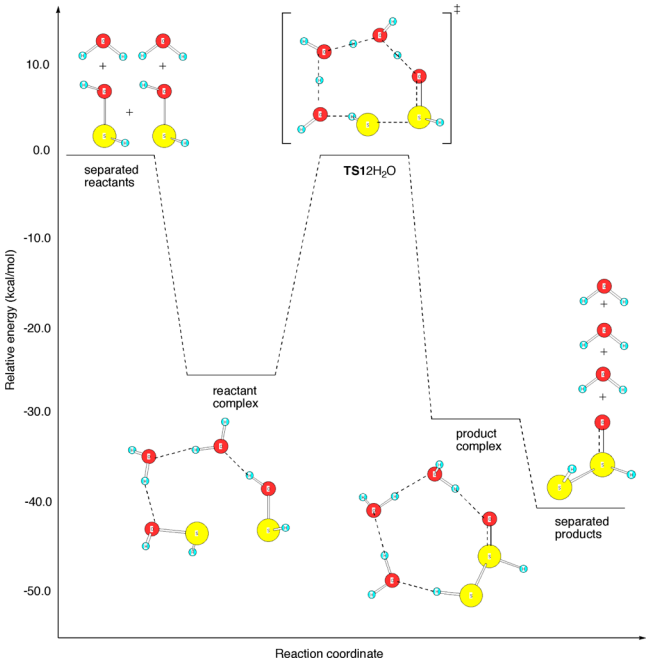


Figure 8. Reaction coordinate for the condensation of hydrogen thioperoxide (**1**) assisted by two explicit water molecules.

connect **TS5** to the *O*-**1**---**7** reactant complex and to the **14**---H_2O product complex. Figure 12 also shows the O-sulfenylation product, sulfenate ester (3*Z*)-4-mercaptooxy-3-penten-2-one (**14**), and its tautomer, substituted *s-cis*-1,3-pentadiene **14a**.

In contrast to C-sulfenylation, in O-sulfenylation the negative charge at O3 in **1** has increased from −0.808 to −0.912 on going to transition state **TS5** (Table SI-5 in the Supporting Information). In **TS5** the negative charge on O2 has decreased from −0.646 in **7** to −0.615, the positive charge at C2 in **7** has increased from 0.462 to 0.525, and the positive charge at C4 has increased from 0.525 to 0.538. It can also be seen in Table SI-5 that the positive charge at S in **1** has increased from 0.250 to 0.259 and the positive charge on the sulfanyl hydrogen (S−H) has increased from 0.087 to 1.111 in **TS5**. The O2−S−O3 bond angle in **TS5** is 152.7°. The transition state structure **TS5** is similar to that predicted for the water-free O-sulfenylation of 1,3-cyclohexanedione by cysteine sulfenic acid.[12]

The data in Table 5 show that the C-sulfenylation reaction is exothermic, that the O-sulfenylation reaction is endothermic, and that the predicted energy barrier for O-sulfenylation is lower than that for C-sulfenylation, as is expected for the formation of a kinetic product. There is better agreement among the levels of theory in predicting the energy barrier for O-sulfenylation than for C-sulfenylation. The relative energies of the C-sulfenylation and O-sulfenylation products and their respective tautomers are given in Table 6. All levels of theory predict sulfide **13** (the thermodynamic product) to be lower in energy than the corresponding isomeric kinetic product **14**, with B3LYP predicting the smallest energy difference between the two products and LC-ωPBE predicting the largest energy difference. The B3LYP-predicted vibrational frequencies of **6** and **7**, the products **13** and **14**, and their respective tautomers **13a**/**13aa** and **14a** are given in Table 7.

As in the predicted condensation and tautomerism mechanisms described above, it was expected that the incorporation of explicit water molecules into the C-sulfenylation and O-sulfenylation mechanisms would relieve strain, stabilize charges, lower energy barriers, and set up proton relay networks of water molecules to facilitate proton transfer from O1 in enolone **7** to O3 in **1** through a Grotthuss-type mechanism.[12−14,78−84] The reactants **1**, **7**, and water lead to the *C*-**1**---**7**---H_2O reactant complex for C-sulfenylation (Figure 13) and the *O*-**1**---**7**---H_2O reactant complex for O-sulfenylation (Figure 14). The *C*-**1**---**7**---H_2O reactant complex is close in energy to the separated reactants, and the *O*-**1**---**7**---H_2O reactant complex is higher in energy than the separated reactants (Table 8). These reactant complexes afford the respective cyclic transition state structures **TS4**H_2O for the C-sulfenylation and **TS5**H_2O for the O-sulfenylation of enolone **7** by hydrogen thioperoxide **1**. The energy barrier $E^{\ddagger}$ for C-sulfenylation in the presence of one explicit water molecule is higher than that for O-sulfenylation in the presence of one water molecule (Table 8). The **13**---$2H_2O$ product complex is lower in energy than the separated reactants and the separated products, while the **14**---$2H_2O$ product complex is higher in energy than the separated reactants but lower in energy than the separated products. IRC calculations connect **TS4**H_2O to the *C*-**1**---**7**---H_2O

DOI: 10.1021/acs.jpca.5b00779
J. Phys. Chem. A 2015, 119, 3500−3517

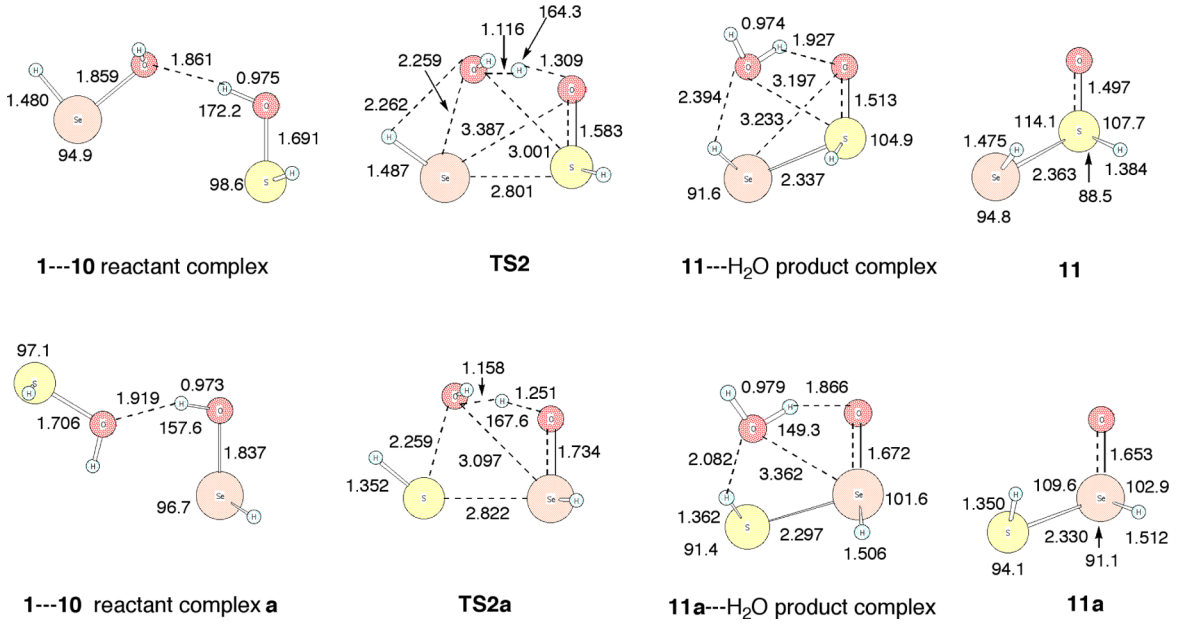


Figure 9. B3LYP-optimized structures of reactant complexes, transition states, product complexes, and products from the condensation of sulfur hydride hydroxide (**1**) with selenium hydride hydroxide (**10**).

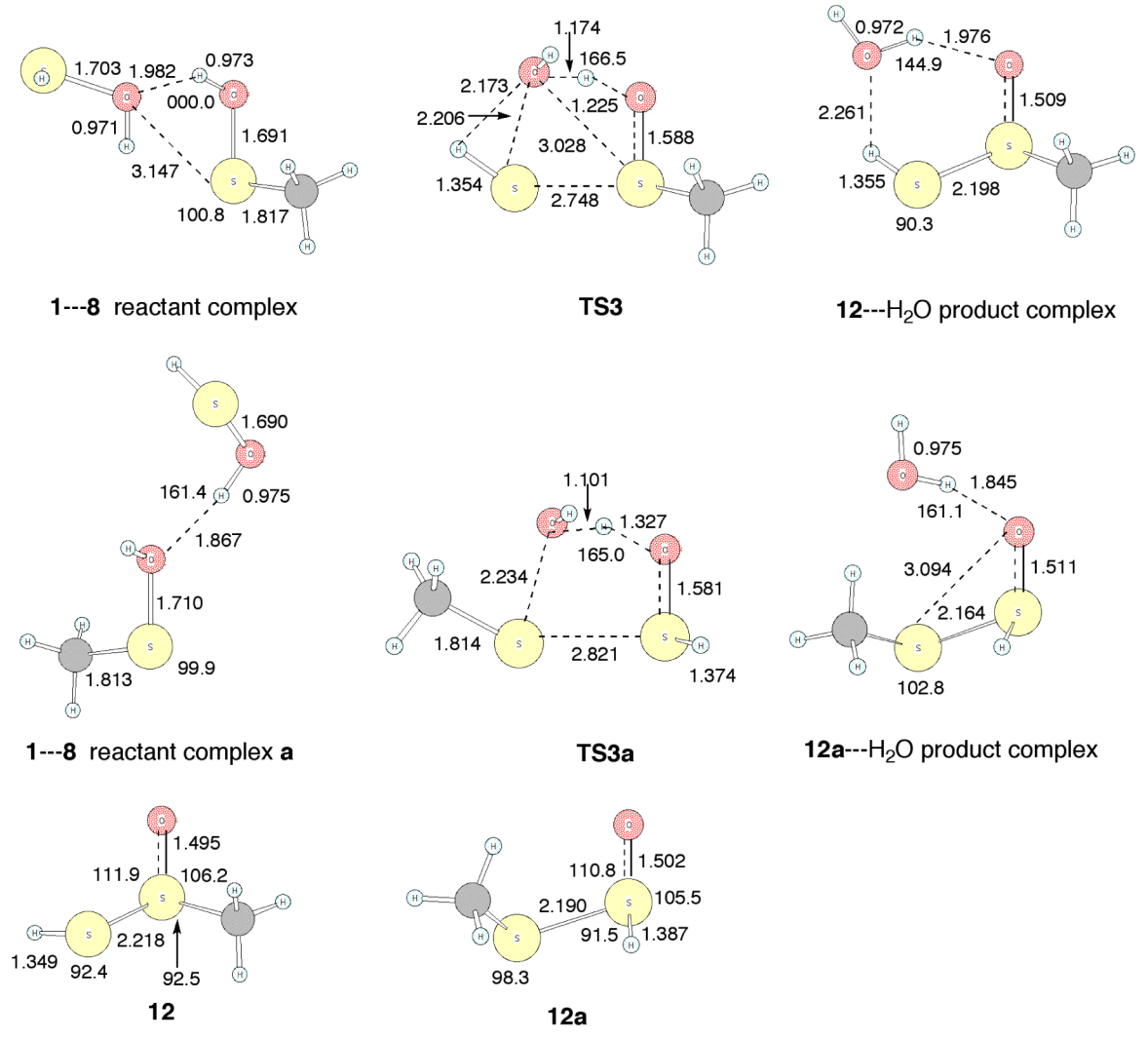


Figure 10. B3LYP-optimized structures of reactant complexes, transition states, product complexes, and products from the condensation of hydrogen thioperoxide (**1**) with methanesulfenic acid (**8**).

DOI: 10.1021/acs.jpca.5b00779
J. Phys. Chem. A 2015, 119, 3500−3517

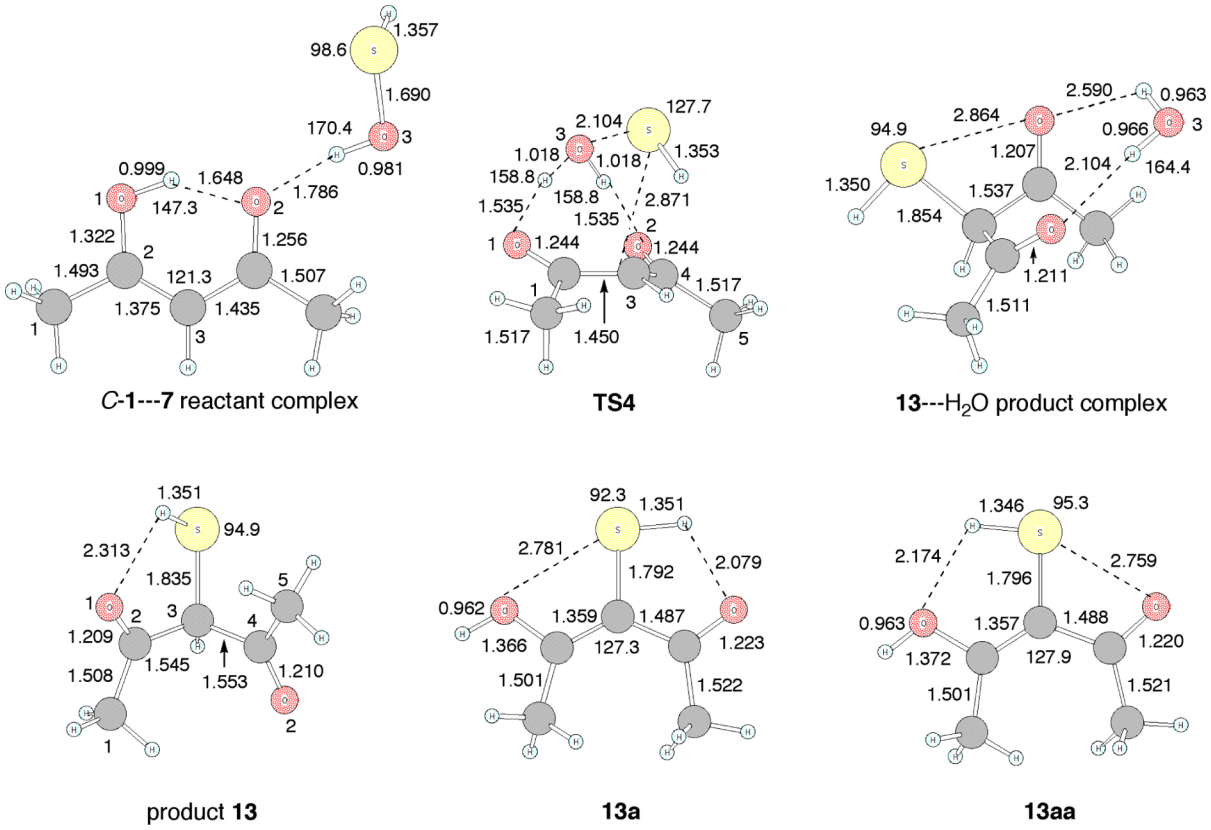


Figure 11. B3LYP-optimized structures of the *C*-**1**---**7** reactant complex, the water-free transition state **TS4**, the **13**---H_2O product complex, product **13**, and two conformations of its tautomer (**13a**, **13aa**) for the C-sulfenylation of enolone **7** with hydrogen thioperoxide (**1**).

Table 5. Comparison of the Relative Energies and Energy Barriers in the C-Sulfenylation and O-Sulfenylation of Enolone 7 by Hydrogen Thioperoxide (1) via Their Respective Water-Free Transition States TS4 and TS5

	C-sulfenylation via **TS4**[b]					O-sulfenylation via **TS5**[c]				
level[a]	ΔE_1[d]	$E_1^{\ddagger}$[e]	ΔE_2[f]	ΔE_3[g]	ΔE_4[h]	ΔE_5[i]	$E_2^{\ddagger}$[j]	ΔE_6[k]	ΔE_7[l]	ΔE_8[m]
B3LYP	−6.6	46.3	−16.7	0.3	−17.0	−2.5	32.9	8.7	−4.3	13.0
B3PW91	−6.0	47.1	−16.8	1.6	−18.4	−1.9	32.5	10.4	−3.6	14.0
PBE1PBE	−7.4	46.3	−19.7	0.1	−19.8	−3.6	30.8	8.8	−4.9	13.7
PBEh1PBE	−7.5	46.0	−19.8	0.0	−19.8	−3.7	30.6	8.4	−5.0	13.5
M06-2X	−8.3	48.3	−24.6	−2.0	−22.6	−4.5	31.2	5.3	−5.8	11.0
LC-ωPBE	−6.6	55.4	−22.5	0.3	−22.7	−2.6	35.9	9.2	−4.4	13.7
CAM-B3LYP	−7.7	50.9	−18.8	−0.7	−18.1	−3.6	33.7	7.8	−5.3	13.1
ωB97XD	−7.9	48.9	−23.5	−0.8	−22.6	−3.7	33.6	7.1	−5.2	12.3

[a] 6-311+G(d,p) basis set. [b] See Figure 11 for the structures. [c] See Figure 12 for the structures. [d] $\Delta E_1 = E_{\text{C-1---7 reactant complex}} - (E_1 + E_7)$. [e] $E_1^{\ddagger} = E_{\text{TS4}} - (E_1 + E_7)$. [f] $\Delta E_2 = E_{\text{13---H}_2\text{O product complex}} - (E_1 + E_7)$. [g] $\Delta E_3 = E_{\text{13---H}_2\text{O product complex}} - (E_{13} + E_{\text{H}_2\text{O}})$. [h] $\Delta E_4 = (E_{13} + E_{\text{H}_2\text{O}}) - (E_1 + E_7)$. [i] $\Delta E_5 = E_{\text{O-1---7 reactant complex}} - (E_1 + E_7)$. [j] $E_2^{\ddagger} = E_{\text{TS5}} - (E_1 + E_7)$. [k] $\Delta E_6 = E_{\text{14---H}_2\text{O product complex}} - (E_1 + E_7)$. [l] $\Delta E_7 = E_{\text{14---H}_2\text{O product complex}} - (E_{14} + E_{\text{H}_2\text{O}})$. [m] $\Delta E_8 = (E_{14} + E_{\text{H}_2\text{O}}) - (E_1 + E_7)$.

reactant complex and the **13**---$2H_2O$ product complex and also connect **TS5**H_2O to the *O*-**1**---**7**---H_2O reactant complex and the **14**---$2H_2O$ product complex. As shown by the data in Table 8, all levels of theory predict that the presence of one water molecule in each mechanism significantly lowers the energy barriers for C-sulfenylation (from 46.3 to ∼28.6 kcal/mol) and O-sulfenylation (from 32.9 to ∼22.0 kcal/mol). It can also be seen in Table 8 that there good agreement among the different levels of theory for predicting the energy barrier for C-sulfenylation and better agreement for predicting the energy barrier for O-sulfenylation.

Figures 13 and 14 show the respective hydrogen-bonding and nonbonding patterns in the reaction complexes, in the C-sulfenylation transition state **TS4**H_2O, and in the O-sulfenylation transition state **TS5**H_2O. In transition state **TS4**H_2O (Figure 13) the explicit water molecule (H_2O-1), which is hydrogen-bonded to O1 and O2, is accepting a proton from O1 while it is transferring one of its protons to O3 to assist in the formation of the water molecule. At the same time, the S−O3 bond is breaking and the S−C3 bond is forming. The transfer of the O1 proton to H_2O-1 increases the electron density at C3, which enhances its nucleophilicity. Table SI-6 in the Supporting Information shows the increase in negative charge at C3 in going from the ground state **7** to **TS4**H_2O. The positive charge on sulfur decreases as it undergoes nucleophilic attack by C3. The hydrogen bonding in **TS4**H_2O is similar to that in the water-free transition state **TS4**

DOI: 10.1021/acs.jpca.5b00779
J. Phys. Chem. A 2015, 119, 3500−3517

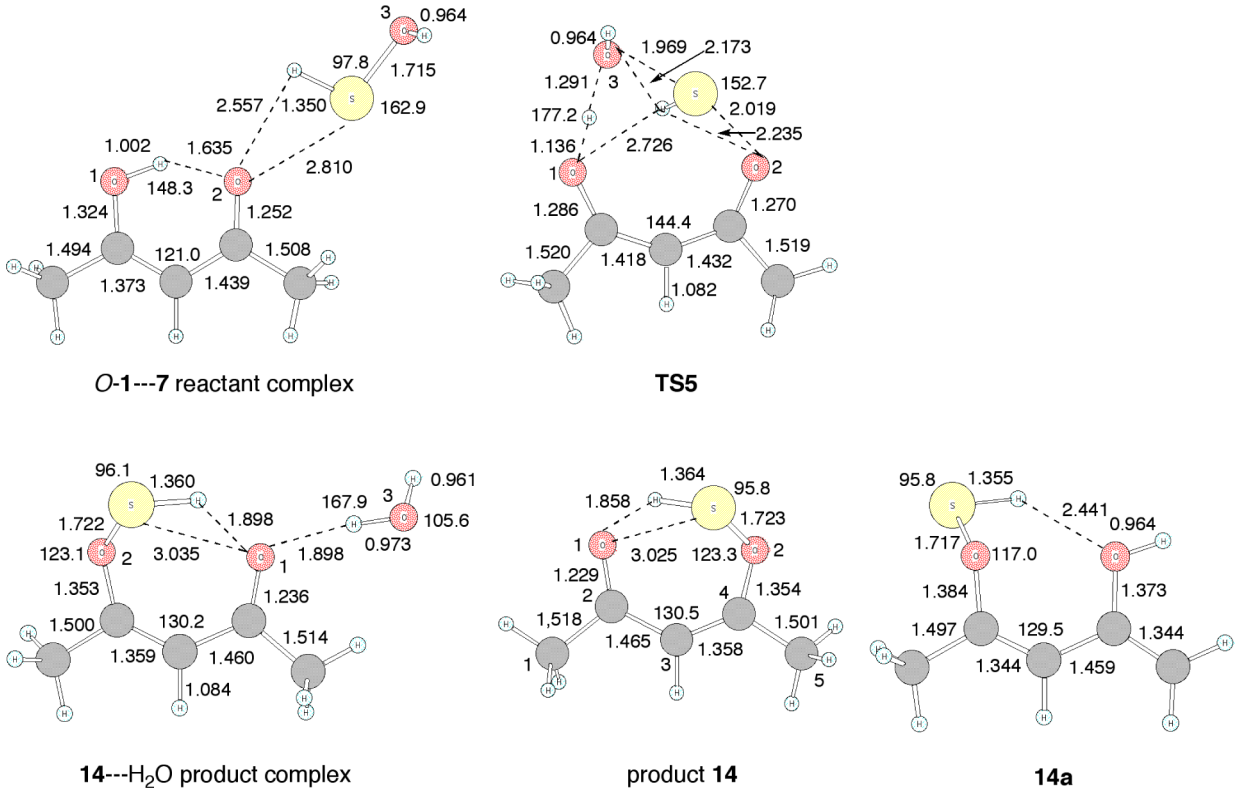


Figure 12. B3LYP-optimized structures of the *O*-**1**---**7** reactant complex, the water-free transition state **TS5**, the **14**---H_2O product complex, product **14**, and its tautomer **14a** for the O-sulfenylation of enolone **7** with hydrogen thioperoxide (**1**).

Table 6. Relative Energies of the Products and Tautomers for C-Sulfenylation (13, 13a, 13aa) and O-Sulfenylation (14, 14a)

level[a]	ΔE_1[b]	ΔE_2[c]	ΔE_3[d]	ΔE_4[e]
B3LYP	10.4	12.1	14.9	30.0
B3PW91	10.2	12.1	15.3	32.3
PBE1PBE	10.2	12.1	15.1	33.5
PBEh1PBE	10.1	12.1	15.2	33.3
M06-2X	11.2	12.6	12.1	33.6
LC-ωPBE	13.7	15.2	16.3	36.4
CAM-B3LYP	11.4	12.9	15.1	31.3
ωB97XD	12.6	14.0	15.8	34.9

[a]6-311+G(d,p) basis set. [b]$\Delta E_1 = E_{13a} - E_{13}$. [c]$\Delta E_2 = E_{13aa} - E_{13}$. [d]$\Delta E_3 = E_{14a} - E_{14}$. [e]$\Delta E_4 = E_{14} - E_{13}$.

(Figure 11). The C3−S−O3 bond angle in **TS4**H_2O is larger than that in the water-free transition state **TS4**, and the S···O3, S···C3, and O1···H distances in **TS4**H_2O are shorter than those in **TS4**.

The changes in geometry and nonbonding interactions in going from the *O*-**1**---**7**---H_2O reactant complex to transition state **TS5**H_2O are shown in Figure 14. The bond distances in **TS5**H_2O are consistent with π-electron delocalization through atoms O1−C2−C3−C4−O2 and the change in the nucleophilic center from C3 to O2. It can be seen in Table SI-6 in the Supporting Information that the negative charge at C3 in **TS4**H_2O is larger in than that in **TS5**H_2O and that the positive charge on sulfur is larger in **TS5**H_2O than in **TS4**H_2O. The O1···C2 distance becomes shorter, and the C2···C3 and O2···C4 distances become longer; the O2−S−O3 bond angle in **TS5**H_2O is almost linear (176.2°). The transfer of the O1 proton is greater in the C-sulfenylation transition state **TS4**H_2O than in the O-sulfenylation transition state **TS5**H_2O.

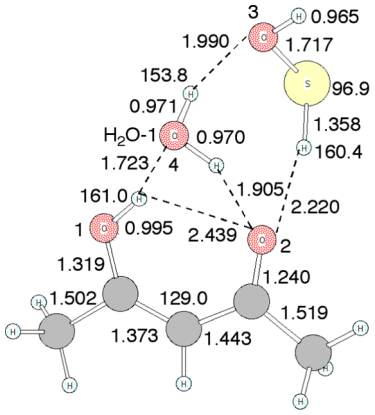
The inclusion of two water molecules in the reaction mechanisms leads to the reaction complexes and transition states for C-sulfenylation and O-sulfenylation shown in

Table 7. Infrared Stretching Frequencies of 2,4-Pentanedione (6), (3*Z*)-4-Hydroxy-3-penten-2-one (7), 3-Mercapto-2,4-pentanedione (13), (3*Z*)-4-Hydroxy-3-mercapto-3-penten-2-one (13a, 13aa), (3*Z*)-4-Mercaptooxy-3-penten-2-one (14), and the *s-cis*-1,3-Pentadiene Derivative 14a[a,b]

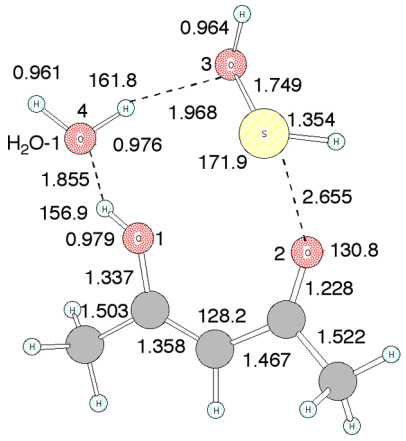
	C=C−C=O_{as}	C=C−C=O_s	C=O_{as}	C=O_s	C−O	S−H	O−H
6[c]			1764 (407)	1794 (23)			
7[c]			1676 (378)	1637 (283)[d]			3067 (354)
13[e]			1765 (336)	1794 (26)		2655 (10)	
13a	1700 (115)	1655 (281)			1259 (40)	2638 (35)	3834 (99)
13aa	1715 (144)	1662 (227)			1249 (55)	2696 (1)	3834 (95)
14	1713 (237)	1610 (386)				2508 (142)	
14a	1712 (126)	1649 (63)				2620 (4)	3824 (42)

[a]Calculated at the B3LYP/6-311+G(d,p) level. [b]Relative intensities are given in parentheses. [c]See also refs 19 and 20. [d]Coupled with the O−H bending vibration. [e]C−S at 835 (3).

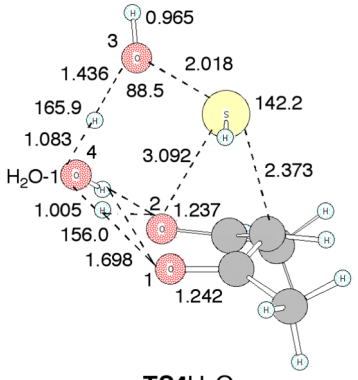
DOI: 10.1021/acs.jpca.5b00779
J. Phys. Chem. A 2015, 119, 3500−3517



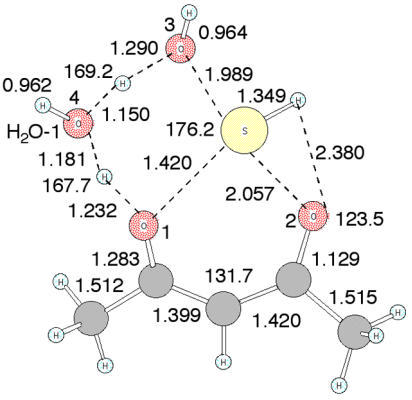
C-**1**---**7**---H_2O reactant complex



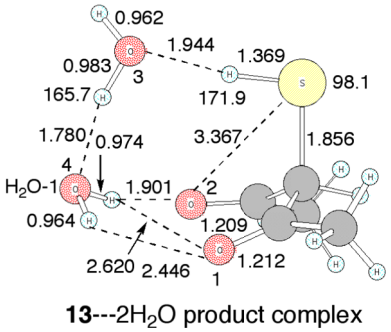
O-**1**---**7**---H_2O-reactant complex



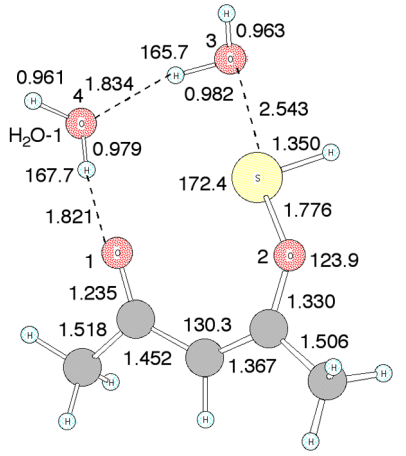
TS4H_2O



TS5H_2O



13---2H_2O product complex



14---2H_2O-product complex

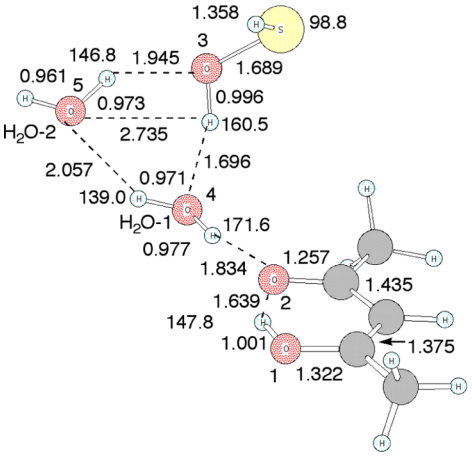
Figure 13. B3LYP-optimized structures of the reactant complex, the transition state **TS4**H_2O, and the product complex in the C-sulfenylation of enolone **7** by hydrogen thioperoxide (**1**) assisted by one explicit water molecule.

Figure 14. B3LYP-optimized structures of the reactant complex, the transition state **TS5**H_2O, and the product complex in the O-sulfenylation of enolone **7** by hydrogen thioperoxide (**1**) assisted by one explicit water molecule.

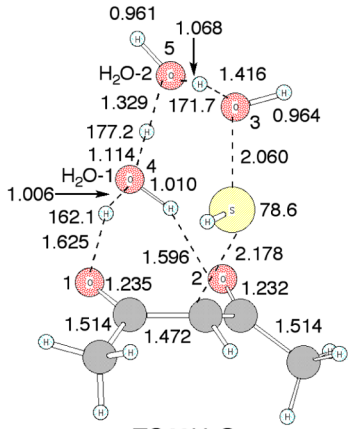
Figures 15 and 16, respectively. The presence of two water molecules in the mechanisms further lowers the energy barriers to C-sulfenylation and to O-sulfenylation, and the energy barrier for O-sulfenylation is higher than that for C-sulfenylation (Table 9). Incorporation of three water molecules into the C-sulfenylation mechanism for **1** and **7** does not significantly change the energy barrier relative to the mechanism involving two water molecules (Figure 17 in the Supporting Information; cf. Table 9 and Table SI 7 in the Supporting Information). The reaction is predicted to be endothermic (nearly thermoneutral), with the *C*-**1**---**7**---3H_2O reactant complex higher in energy than the separated reactants. Incorporation of three water molecules in the O-sulfenylation mechanism for **1** and **7** increases in the energy barrier relative to the mechanism involving two water molecules, and the *O*-**1**---**7**---3H_2O reactant complex is higher in energy than the separated reactants (Figure 18 in the Supporting Information; cf. Table 9 and Table SI 7 in the Supporting Information).

At the B3LYP/6-311+G(d,p) level, the decrease in entropy in going from the respective reactants to the transition state structures for the C-sulfenylation and O-sulfenylation of

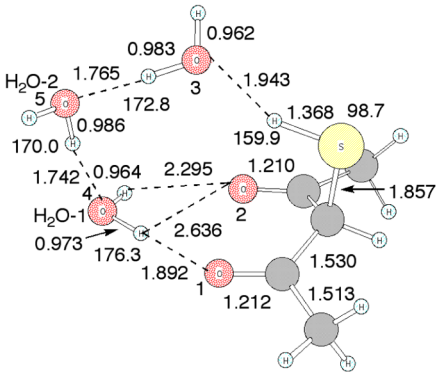
DOI: 10.1021/acs.jpca.5b00779
J. Phys. Chem. A 2015, 119, 3500−3517



C-**1**---**7**---2H_2O reactant complex

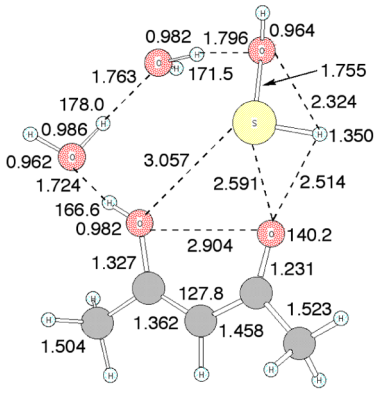


TS42H_2O

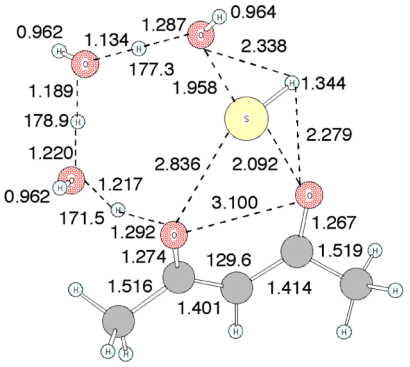


13---3H_2O product complex

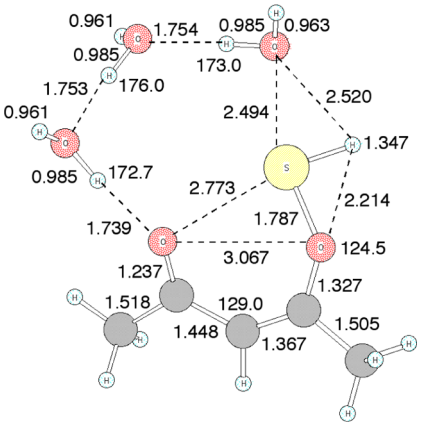
Figure 15. B3LYP-optimized structures of the reactant complex, the transition state **TS4**2H_2O, and the product complex in the C-sulfenylation of enolone 7 by hydrogen thioperoxide (**1**) assisted by two explicit waters.



O-**1**---**7**---2H_2O reactant complex



TS52H_2O



14---3H_2O product complex

Figure 16. B3LYP-optimized structures of the reactant complex, the transition state **TS5**2H_2O, and the product complex in the O-sulfenylation of enolone 7 by hydrogen thioperoxide (**1**) assisted by two explicit water molecules.

2,4-pentanedione (**6**) through its enol tautomer 7 by hydrogen thioperoxide **1** are similar. In C-sulfenylation, the decrease in entropy in going from the reactants to the water-free transition state is 39.7 eu, and successive additions of the first, second, and third water molecules to the transition state add 20.7, 16.0, and 15.3 eu, respectively. Similarly, in O-sulfenylation the decrease in entropy for the water-free transition state relative to the reactants is 40.8 eu, and successive additions of the first, second, and third water molecules to the transition state add 20.7, 16.4, and 15.3 eu, respectively.

CONCLUSIONS

The mechanisms of the tautomerization, condensations, and C-sulfenylation and O-sulfenylation of 2,4-pentanedione by sulfur hydride hydroxide (hydrogen thioperoxide, oxadisulfane) have been studied using 11 different levels of theory. Similar mechanistic trends and reaction pathways are observed among the mechanisms of the three reactions.

DOI: 10.1021/acs.jpca.5b00779
J. Phys. Chem. A 2015, 119, 3500−3517

Table 8. Relative Thermodynamic Parameters, Relative Energies, and Energy Barriers in the C-Sulfenylation and O-Sulfenylation of Enolone 7 by Hydrogen Thioperoxide (1) via Their Respective Water-Assisted Transition States TS4H_2O and TS5H_2O

	C-sulfenylation via **TS4**H_2O[b]					O-sulfenylation via **TS5**H_2O[c]				
level[a]	ΔE_1[d]	$E_1^{\ddagger}$[e]	ΔE_2[f]	ΔE_3[g]	ΔE_4[h]	ΔE_5[i]	$E_2^{\ddagger}$[j]	ΔE_6[k]	ΔE_7[l]	ΔE_8[m]
B3LYP	0.3	28.6	−22.1	−10.3	−11.9	10.1	22.0	7.3	−10.9	18.2
B3PW91	2.0	27.7	−22.1	−8.5	−13.6	12.4	22.4	9.5	−9.2	18.7
PBE1PBE	−0.2	24.2	−25.5	−11.7	−13.8	10.0	20.5	7.3	−12.4	19.7
PBEh1PBE	−0.4	24.7	−25.7	−12.0	−13.7	9.7	20.1	6.8	−12.7	19.6
M06-2X	−3.7	22.7	−28.9	−12.8	−16.1	4.8	20.1	3.0	−14.5	17.5
LC-ωPBE	−1.8	30.3	−27.3	−10.0	−17.3	2.8	26.8	8.8	−10.3	19.1
CAM-B3LYP	−1.1	29.4	−24.6	−12.7	−11.9	8.9	22.5	6.5	−12.9	19.3
ωB97XD	−2.6	28.1	−29.4	−12.9	−16.5	0.1	23.6	5.9	−12.5	18.4

[a]6-311+G(d,p) basis set. [b]See Figure 13 for the structures. [c]See Figure 14 for the structures. [d]$\Delta E_1 = E_{\text{C-1---7---H}_2\text{O reactant complex}} - (E_1 + E_7 + E_{H_2O})$. [e]$E_1^{\ddagger} = E_{\text{TS4H}_2\text{O}} - (E_1 + E_7 + E_{H_2O})$. [f]$\Delta E_2 = E_{\text{13---2H}_2\text{O product complex}} - (E_1 + E_7 + E_{H_2O})$. [g]$\Delta E_3 = E_{\text{13---2H}_2\text{O product complex}} - (E_{13} + 2E_{H_2O})$. [h]$\Delta E_4 = (E_{13} + 2E_{H_2O}) - (E_1 + E_7 + E_{H_2O})$. [i]$\Delta E_5 = E_{\text{O-1---7---H}_2\text{O reactant complex}} - (E_1 + E_7 + E_{H_2O})$. [j]$E_2^{\ddagger} = E_{\text{TS5H}_2\text{O}} - (E_1 + E_7 + E_{H_2O})$. [k]$\Delta E_6 = E_{\text{14---2H}_2\text{O product complex}} - (E_1 + E_7 + E_{H_2O})$. [l]$\Delta E_7 = E_{\text{14---2H}_2\text{O product complex}} - (E_{14} + 2E_{H_2O})$. [m]$\Delta E_8 = (E_{14} + 2E_{H_2O}) - (E_1 + E_7 + E_{H_2O})$.

Table 9. Relative Thermodynamic Parameters, Relative Energies, and Energy Barriers in the C-Sulfenylation and O-Sulfenylation of Enolone 7 by Hydrogen Thioperoxide (1) via Their Respective Two-Water Transition States TS42H_2O and TS52H_2O

	C-sulfenylation via **TS42**H_2O[b]					O-sulfenylation via **TS52**H_2O[c]				
level[a]	ΔE_1[d]	$E_1^{\ddagger}$[e]	ΔE_2[f]	ΔE_3[g]	ΔE_4[h]	ΔE_5[i]	$E_2^{\ddagger}$[j]	ΔE_6[k]	ΔE_7[l]	ΔE_8[m]
B3LYP	−5.5	14.8	−21.3	−17.2	−4.1	5.5	18.0	5.8	−20.1	25.9
B3PW91	−4.9	12.9	−21.5	−14.8	−6.7	7.6	17.9	7.8	−17.9	25.6
PBE1PBE	−6.5	10.0	−24.7	−19.3	−5.4	5.4	15.9	5.8	−22.3	28.1
PBEh1PBE	−6.6	9.8	−24.7	−19.7	−5.0	15.8	15.9	5.4	−22.9	28.3
M06-2X	−8.3	7.9	−27.5	−20.4	−7.1	1.6	15.9	2.9	−23.6	26.5
LC-ωPBE	−5.5	16.3	−26.3	−16.7	−9.5	6.5	22.3	7.6	−19.2	26.9
CAM-B3LYP	−6.5	15.2	−23.3	−20.6	−2.7	4.7	18.2	5.4	−23.1	28.6
ωB97XD	−7.4	12.7	−28.0	−20.1	−7.8	3.5	20.0	4.8	−22.4	27.1

[a]6-311+G(d,p) basis set. [b]See Figure 15 for the structures. [c]See Figure 16 for the structures. [d]$\Delta E_1 = E_{\text{C-1---7---2H}_2\text{O reactant complex}} - (E_1 + E_7 + 2E_{H_2O})$. [e]$E_1^{\ddagger} = E_{\text{TS42H}_2\text{O}} - (E_1 + E_7 + 2E_{H_2O})$. [f]$\Delta E_2 = E_{\text{13---3H}_2\text{O product complex}} - (E_1 + E_7 + 2E_{H_2O})$. [g]$\Delta E_3 = E_{\text{13---3H}_2\text{O product complex}} - (E_{13} + 3E_{H_2O})$. [h]$\Delta E_4 = (E_{13} + 3E_{H_2O}) - (E_1 + E_7 + 2E_{H_2O})$. [i]$\Delta E_5 = E_{\text{O-1---7---2H}_2\text{O reactant complex}} - (E_1 + E_7 + 2E_{H_2O})$. [j]$E_2^{\ddagger} = E_{\text{TS52H}_2\text{O}} - (E_1 + E_7 + 2E_{H_2O})$. [k]$\Delta E_6 = E_{\text{14---3H}_2\text{O product complex}} - (E_1 + E_7 + 2E_{H_2O})$. [l]$\Delta E_7 = E_{\text{14---3H}_2\text{O product complex}} - (E_{14} + 3E_{H_2O})$. [m]$\Delta E_8 = (E_{14} + 3E_{H_2O}) - (E_1 + E_7 + 2E_{H_2O})$.

The tautomerism of the more stable sulfenyl tautomer of hydrogen thioperoxide to its less stable sulfinyl tautomer in the gas phase involves the transfer of a hydrogen from oxygen to sulfur through a cyclic three-center transition state (**TS**, CCSD(T) activation energy barrier $E^{\ddagger}$ = 65.1 kcal/mol). Incorporation of one water molecule (**TS**H_2O, $E^{\ddagger}$ = 31.1 kcal/mol), two water molecules (**TS**2H_2O, $E^{\ddagger}$ = 14.5 kcal/mol), or three water molecules (**TS**3H_2O, $E^{\ddagger}$ = 5.6 kcal/mol) into the mechanism lowers the activation energy barrier. The explicit water molecules set up proton relay networks that reduce ring strain, generate favorable conformations for reactivity, lower energy barriers, and increase the numbers of stabilizing hydrogen bonds and nonbonding interactions. The tautomerism mechanisms with water molecules involve hydrogen-bonding- and nonbonding-stabilized reactant complexes and product complexes.

The CCDS(T)-predicted energy barriers for the condensation of hydrogen thioperoxide to form thiosulfinic acid (sulfinothioic acid) through water-free, one-water, and two-water transition states are $E^{\ddagger}$ = 42.0, 18.3, and ∼0 kcal/mol, respectively. Hydrogen thioperoxide is predicted to undergo condensation with selenium hydride hydroxide to afford isomeric products containing sulfur−selenium bonds. Hydrogen thioperoxide is also predicted to undergo condensation with methanesulfenic acid to give methanesulfinothioic acid and hydro(methanethiolato)-oxosulfur.

Hydrogen thioperoxide is predicted to add to the lower-energy tautomer (enolone, ketoenol) of 2,4-pentanedione to form C-sulfenylated (sulfide, thioether, **TS4**, $E^{\ddagger}$ = 46.3 kcal/mol) and O-sulfenylated (**TS5**, sulfenate ester, $E^{\ddagger}$ = 32.9 kcal/mol) products. In the water-free mechanisms, the reactions occur through two independent paths involving different reactant complexes that are lower in energy than the separated reactants. In the mechanism through the water-free transition state, the sulfide is the thermodynamic product and the sulfenate ester is the kinetic product. The energy barriers for C-sulfenylation ($E^{\ddagger}$ = 28.6 kcal/mol) and O-sulfenylation ($E^{\ddagger}$ = 22.0 kcal/mol) are lower and the energy barrier for C-sulfenylation is predicted to be higher than that for O-sulfenylation when one explicit water molecule in included in the mechanisms. Incorporation of two explicit water molecules in the mechanisms lowers the $E^{\ddagger}$ for C-sulfenylation to 14.8 kcal/mol and $E^{\ddagger}$ for O-sulfenylation to 18.0 kcal/mol. Inclusion of three explicit water molecules in the mechanisms does not significantly change energy barrier for C-sulfenylation but increases the energy barrier for O-sulfenylation, making it larger than the predicted C-sulfenylation energy barrier. Thus, incorporation of two water molecules in the mechanisms appears to the best model for each reaction.

DOI: 10.1021/acs.jpca.5b00779
J. Phys. Chem. A 2015, 119, 3500−3517

■ ASSOCIATED CONTENT

Supporting Information

Tables of energy barriers and relative energies for condensation reactions; tables of atomic charges of reactants and transition states; and tables of energy barriers and relative energies and figures showing structures of reactant and product complexes and transition states for C-sulfenylation and O-sulfenylation of 2,4-pentanedione assisted by three water molecules. This material is available free of charge via the Internet at http://pubs.acs.org.

■ AUTHOR INFORMATION

Corresponding Author

*Tel: 949-824-6501. E-mail: ffreeman@uci.edu.

Notes

The authors declare no competing financial interest.

■ ACKNOWLEDGMENTS

We thank the National Science Foundation for NSF CHE-0840513 that supports the Greenplanet Computing Cluster at the University of California, Irvine.

■ REFERENCES

(1) Smardzewski, R. R.; Lin, M. C. Matrix Reactions of Oxygen with H_2S Molecules. *J. Chem. Phys.* **1977**, *66*, 3197−3204.
(2) Iraqi, M.; Schwarz, H. Experimental Evidence for the Gas Phase Existence of HSOH (Hydrogen Thioperoxide) and SOH_2 (Thiooxonium Ylide). *Chem. Phys. Lett.* **1994**, *221*, 359−362.
(3) Besnainou, S.; Whitten, J. L. Intermediate Molecular Species in the Oxidation of H_2S. An ab Initio Configuration Interaction Study. *J. Am. Chem. Soc.* **1980**, *102*, 7444−7448.
(4) Vahedpour, M.; Baghary, R.; Khalili, F. Prediction of Mechanism and Thermochemical Properties of O_3 + H_2S Atmospheric Reaction. *J. Chem.* **2013**, No. 659682.
(5) Grant, D. J.; Dixon, D. A.; Francisco, J. S.; Feller, D.; Peterson, K. A. Heats of Formation of the $H_{1,2}O_mS_n$ (m, n = 0−3) Molecules from Electronic Structure Calculations. *J. Phys. Chem. A* **2009**, *113*, 11343−11353.
(6) Cárdenas-Jirón, G. I.; Letelier, J. R.; Toro-Labbé, A. The Internal Rotation of Hydrogen Thioperoxide: Energy, Chemical Potential, and Hardness Profiles. *J. Phys. Chem. A* **1998**, *102*, 7864−7871.
(7) Winnewisser, G.; Lewen, F.; Thorwirth, S.; Behnke, M.; Hahn, J.; Gauss, J.; Herbst, E. Gas-Phase Detection of HSOH: Synthesis by Flash Vacuum Pyrolysis of Di-*tert*-butyl Sulfoxide and Rotational−Torsional Spectrum. *Chem.—Eur. J.* **2003**, *9*, 501−510.
(8) Beckers, H.; Esser, S.; Metzroth, T.; Behnke, M.; Willner, H.; Gauss, J.; Hahn, J. Low-Pressure Pyrolysis of *t*-Bu_2SO: Synthesis and IR Spectroscopic Detection of HSOH. *Chem.—Eur. J.* **2006**, *12*, 832−844.
(9) Davis, F. A.; Billmers, R. L. Chemistry of Sulfenic Acids. 6. Structures of Simple Sulfenic Acids Generated by Flash Vacuum Pyrolysis. *J. Org. Chem.* **1985**, *50*, 2593−2595.
(10) Alkorta, I.; Elguero, J. Classical versus Redox Tautomerism: Substituent Effects on the Keto/Enol and Sulfoxide/Sulfenic Acid Equilibria. *Tetrahedron Lett.* **2004**, *45*, 4127−4129.
(11) Freeman, F.; Bui, A.; Dinh, L.; Hehre, W. J. Dehydrative Cyclocondensation Mechanisms of Hydrogen Thioperoxide and of Alkanesulfenic Acids. *J. Phys. Chem. A* **2012**, *116*, 8031−8039.
(12) Freeman, F. Mechanism of the Cysteine Sulfenic Acid *O*-Sulfenylation of 1,3-Cyclohexanedione. *Chem. Commun.* **2014**, *50*, 4102−4104.
(13) Freeman, F.; Adesina, I. T.; La, J. L.; Lee, J. Y.; Poplawski, A. A. Conformers of Cysteine and Cysteine Sulfenic Acid and Mechanisms of the Reaction of Cysteine Sulfenic Acid with 5,5-Dimethyl-1,3-cyclohexanedione (Dimedone). *J. Phys. Chem. B* **2013**, *117*, 16000−16012.
(14) Wagner, G. Mechanistic Aspects of the Reaction of Dimedone Derivatives with Sulfenic Acids and Other Sulfur Compounds—A Computational Study. *Tetrahedron* **2013**, *69*, 7243−7252.
(15) Gupta, V.; Carroll, K. S. Sulfenic Acid Chemistry, Detection and Cellular Lifetime. *Biochim. Biophys. Acta* **2014**, *1840*, 847−875.
(16) Furdui, C. M.; Poole, L. B. Chemical Approaches To Detect and Analyze Protein Sulfenic Acids. *Mass Spectrom. Rev.* **2014**, *33*, 126−146.
(17) Rudyk, O.; Eaton, P. Biochemical Methods for Monitoring Protein Thiol Redox States in Biological Systems. *Redox Biol.* **2014**, *2*, 803−813.
(18) Mikolajczyk, M.; Cypryk, M.; Krasiński, G. Quantum Chemical Study of Thiosulfinic Acids and Their Anions. *J. Mol. Struct: THEOCHEM* **2008**, *863*, 105−110.
(19) Steudel, R.; Drozdova, Y.; Hertwig, R. H.; Koch, W. Structures, Energies, and Vibrational Spectra of Several Isomeric Forms of H_2S_2O and Me_2S_2O: An *ab Initio* Study. *J. Phys. Chem.* **1995**, *99*, 5319−5324.
(20) Li, H.; O'Connor, P. B. Electron Capture Dissociation of Disulfide, Sulfur−Selenium, and Diselenide Bound Peptides. *J. Am. Soc. Mass Spectrom.* **2012**, *23*, 2001−2010.
(21) Wessjohann, L. A.; Schneider, A. Synthesis of Selenocysteine and Its Derivatives with an Emphasis on Selenylsulfide (−Se−S−) Formation. *Chem. Biodiversity* **2008**, *5*, 375−388.
(22) Luo, G.; Ren, X.; Liu, J.; Mu, Y.; Shen, J. Toward More Efficient Glutathione Peroxidase Mimics: Substrate Recognition and Catalytic Group Assembly. *Curr. Med. Chem.* **2003**, *10*, 1151−1183.
(23) Tiecco, M.; Santoro, S.; Santi, C. The Nature of Nonbonded Interactions between Divalent Selenium and Sulfur: A Theoretical Investigation. In *Proceedings of the 15th International Electronic Conference on Synthetic Organic Chemistry, 1−30 November 2011*; Sciforum Electronic Conference Series, Vol. *15*; MDPI AG: Basel, Switzerland, 2011.
(24) Belova, N. V.; Oberhammer, H.; Trang, N. H.; Girichev, G. V. Tautomeric Properties and Gas-Phase Structure of Acetylacetone. *J. Org. Chem.* **2014**, *79*, 5412−5419.
(25) Srinivasa, R.; Feenstra, J. S.; Park, S. T.; Xu, S.; Zewail, A. H. Direct Determination of Hydrogen-Bonded Structures in Resonant and Tautomeric Reactions Using Ultrafast Electron Diffraction. *J. Am. Chem. Soc.* **2004**, *126*, 2266−2267.
(26) Alagona, G.; Ghio, C. Keto−Enol Tautomerism in Linear and Cyclic β-Diketones: A DFT Study in Vacuo and in Solution. *Int. J. Quantum Chem.* **2008**, *108*, 1840−1855.
(27) Iijima, K.; Ohnogi, A.; Shibata, S. The Molecular Structure of Acetylacetone As Studied by Gas-Phase Electron Diffraction. *J. Mol. Struct.* **1957**, *156*, 111−118.
(28) Boese, R.; Antipin, M. Y.; Bläser, D.; Lyssenko, K. A. Molecular Crystal Structure of Acetylacetone at 210 and 110 K: Is the Crystal Disorder Static or Dynamic? *J. Phys. Chem. B* **1998**, *102*, 8654−8660.
(29) (a) Yamabe, S.; Tsuchida, N.; Miyajima, K. Reaction Paths of Keto−Enol Tautomerism in β-Diketones. *J. Phys. Chem. A* **2004**, *108*, 2750−2757. (b) Yamabe, S.; Tsuchida, N. A Computational Study of Interactions between Acetic Acid and Water Molecules. *J. Comput. Chem.* **2003**, *24*, 939−947.
(30) Frisch, M. J.; Trucks, G. W.; Schlegel, H. B.; Scuseria, G. E.; Robb, M. A.; Cheeseman, J. R.; Montgomery, J. A., Jr.; Vreven, T.; Kudin, K. N.; Burant, J. C., et al. *Gaussian 03*, revision A.1; Gaussian, Inc.: Wallingford, CT, 2004.
(31) (a) Kong, J.; White, C. A.; Krylov, A. I.; Sherrill, C. D.; Adamson, R. D.; Furlani, T. R.; Lee, M. S.; Lee, A. M.; Gwaltney, S. R.; Adams, T. R.; et al. *J. Comput. Chem.* **2000**, *21*, 1532−1548. (b) Spartan'08 (Wavefunction, Inc., Irvine, CA 92612, 2006) in collaboration with Q-Chem, Inc (Export, PA 15632).
(32) Becke, A. D. Density-Functional Thermochemistry. III. The Role of Exact Exchange. *J. Chem. Phys.* **1993**, *98*, 5648−5652.
(33) Burke, K.; Perdew, J. P.; Wang, Y. In *Electronic Density Functional Theory: Recent Progress and New Directions*; Dobson, J. F., Vignale, G., Das, M. P., Eds.; Plenum Press: New York, 1998.
(34) Burke, K.; Perdew, J. P.; Ernzerhof, M. Generalized Gradient Approximation Made Simple. *Phys. Rev. Lett.* **1996**, *77*, 3865−3868.

DOI: 10.1021/acs.jpca.5b00779
J. Phys. Chem. A 2015, 119, 3500−3517

(35) Adamo, C.; Barone, V. Toward Reliable Density Functional Methods without Adjustable Parameters: The PBE0 Model. *J. Chem. Phys.* **1999**, *110*, 6158−6169.
(36) Burke, K.; Perdew, J. P.; Ernzerhof, M. Generalized Gradient Approximation Made Simple [Phys. Rev. Lett. 77, 3865 (1996)]. *Phys. Rev. Lett.* **1997**, *78*, 1396.
(37) Ernzerhof, M.; Perdew, J. P. Generalized Gradient Approximation to the Angle- and System-Averaged Exchange Hole. *J. Chem. Phys.* **1998**, *109*, 3313−3320.
(38) Zhao, Y.; Truhlar, D. G. Comparative DFT Study of van der Waals Complexes: Rare-Gas Dimers, Alkaline-Earth Dimers, Zinc Dimer, and Zinc−Rare Gas Dimers. *J. Phys. Chem. A* **2006**, *110*, 5121−5129.
(39) Zhao, Y.; Truhlar, D. G. Density Functional Theory for Reaction Energies: Test of Meta and Hybrid Meta Functionals, Range-Separated Functionals, and Other High-Performance Functionals. *J. Chem. Theory Comput.* **2011**, *7*, 669−676.
(40) Vydrov, O. A.; Scuseria, G. E.; Perdew, J. P. Tests of Functionals for Systems with Fractional Electron Number. *J. Chem. Phys.* **2007**, *126*, No. 154109.
(41) Yanai, T.; Tew, D.; Handy, N. C. A New Hybrid Exchange−Correlation Functional Using the Coulomb-Attenuating Method (CAM-B3LYP). *Chem. Phys. Lett.* **2004**, *393*, 51−57.
(42) Chai, J.-D.; Head-Gordon, M. Systematic Optimization of Long-Range Corrected Hybrid Density Functionals. *J. Chem. Phys.* **2008**, *128*, No. 084106.
(43) Bartlett, R. J.; Purvis, G. D., III. Many-Body Perturbation Theory, Coupled-Pair Many-Electron Theory, and Importance of Quadruple Excitations for Correlation Problem. *Int. J. Quantum Chem.* **1978**, *14*, 561−581.
(44) Pople, J. A.; Krishnan, R.; Schlegel, H. B.; Binkley, J. S. Electron Correlation Theories and Their Applications to the Study of Simple Reaction Potential Surfaces. *Int. J. Quantum Chem.* **1978**, *14*, 545−560.
(45) Pople, J. A.; Head-Gordon, M.; Raghavachari, K. Quadratic Configuration Interaction—A General Technique for Determining Electron Correlation Energies. *J. Chem. Phys.* **1987**, *87*, 5968−5975.
(46) Kobayashi, R.; Handy, N. C.; Amos, R. D.; Trucks, G. W.; Frisch, M. J.; Pople, J. A. Gradient Theory Applied to the Bueckner Doubles Method. *J. Chem. Phys.* **1991**, *95*, 6723−6733.
(47) Wilson, A. K.; van Mourik, T.; Dunning, T. H., Jr. Gaussian Basis Sets for Use in Correlated Molecular Calculations. VI. Sextuple Zeta Correlation Consistent Basis Sets for Boron through Neon. *J. Mol. Struct.: THEOCHEM* **1996**, *388*, 339−349 and references therein.
(48) Merrick, J. P.; Moran, D.; Radom, L. An Evaluation of Harmonic Vibrational Frequency Scale Factors. *J. Phys. Chem. A* **2007**, *111*, 11683−11700.
(49) Fábri, C.; Szidarovszky, T.; Magyafalvi, G.; Tarczay, G. Gas-Phase and Ar-Matrix SQM Scaling Factors for Various DFT Functionals with Basis Sets Including Polarization and Diffuse Functions. *J. Phys. Chem. A* **2011**, *115*, 4640−4649.
(50) Gonzalez, C.; Schlegel, H. B. Reaction Path Following in Mass-Weighted Internal Coordinates. *J. Phys. Chem.* **1990**, *94*, 5523−5527.
(51) Reed, A. E.; Curtiss, L. A.; Weinhold, F. Intermolecular Interactions from a Natural Bond Orbital, Donor−Acceptor Viewpoint. *Chem. Rev.* **1988**, *88*, 899 and references therein.
(52) Papajak, E.; Xu, Z. X.; Leverentz, H. R.; Truhlar, D. G. Perspectives on Basis Sets Beautiful: Seasonal Plantings of Diffuse Basis Functions. *J. Chem. Theory Comput.* **2011**, *7*, 3027−3034.
(53) Kruse, H.; Goerigk, L.; Grimme, S. Why the Standard B3LYP/6-31G* Model Chemistry Should Not Be Used in DFT Calculations of Molecular Thermochemistry: Understanding and Correcting the Problem. *J. Org. Chem.* **2012**, *77*, 10824−10834.
(54) Xu, X.; Alecu, I. M.; Truhlar, D. G. How Well Can Modern Density Functionals Predict Internuclear Distances at Transition States? *J. Chem. Theory Comput.* **2011**, *7*, 1667−1676.
(55) Grimme, S.; Steinmetz, M. Effects of London Dispersion Correction in Density Functional Theory on the Structures of Organic Molecules in the Gas Phase. *Phys. Chem. Chem. Phys.* **2013**, *15*, 16031−16042.
(56) Majerz, I. Directionality of Inter- and Intramolecular OHO Hydrogen Bonds: DFT Study Followed by AIM and NBO Analysis. *J. Phys. Chem. A* **2012**, *116*, 7992−8000.
(57) Wendler, K.; Thar, J.; Zahn, S.; Kirchner, B. Estimating the Hydrogen Energy. *J. Phys. Chem. A* **2010**, *114*, 9529−9536.
(58) Cioslowski, J.; Surján, P. R. An Observable-Based Interpretation of Electronic Wavefunctions: Applications to "Hypervalent" Molecules. *J. Mol. Struct.: THEOCHEM* **1992**, *255*, 9−33.
(59) Dobado, J. A.; Martínez-Garcia, H.; Molina, J. M.; Sundberg, M. R. Chemical Bonding in Hypervalent Molecules Revised. 2. Application of the Atoms in Molecules Theory to Y_2XZ and Y_2XZ_2 (Y = H, F, CH_3; X = O, S, Se; Z = O, S) Compounds. *J. Am. Chem. Soc.* **1999**, *121*, 3156−3164.
(60) Cubbage, J. W.; Jenks, W. S. Computational Studies of the Ground and Excited State Potentials of DMSO and H_2SO: Relevance to Photostereomutation. *J. Phys. Chem. A* **2001**, *105*, 10588−10595.
(61) Chestnut, D. B.; Quin, L. D. Nature of Bonding in the Sulfuryl Group. *J. Comput. Chem.* **2004**, *25*, 734−738.
(62) Reed, A. E.; Schleyer, P. v. R. Chemical Bonding in Hypervalent Molecules. The Dominance of Ionic Bonding and Negative Hyperconjugation over d-Orbital Participation. *J. Am. Chem. Soc.* **1990**, *112*, 1434−1445.
(63) Love, I. Polar Covalent Bonds: An AIM Analysis of S,O Bonds. *J. Phys. Chem. A* **2009**, *113*, 2640−2646.
(64) Gutiérrez-Oliva, S.; Letelier, J. R.; Toro-Abbé, A. Energy, Chemical Potential and Hardness Profiles for the Rotational Isomerization of HOOH, HSOH, and HSSH. *Mol. Phys.* **1999**, *96*, 61−70.
(65) Denis, P. A. Theoretical Characterization of the HSOH, H_2SO, and H_2OS Isomers. *Mol. Phys.* **2008**, *106*, 2557−2567.
(66) Sánchez-Sanz, G.; Alkorta, I.; Elguero, J. Theoretical Study of the HXYH Dimers (X, Y = O, S, Se). Hydrogen Bonding and Chalcogen−Chalcogen Interactions. *Mol. Phys.* **2011**, *109*, 2543−2552.
(67) Glendening, E. D.; Shrout, A. L. Influence of Resonance on the Acidity of Sulfides, Sulfoxides, Sulfones, and Their Group 16 Congeners. *J. Phys. Chem. A* **2005**, *109*, 4966−4972.
(68) Poater, J.; Solà, M.; Duran, M.; Fradera, X. New Insights in Chemical Reactivity by Means of Electron Pairing Analysis. *J. Phys. Chem. A* **2001**, *105*, 2052−2063.
(69) Thomas, R.; Shoemaker, C. B.; Eriks, K. The Molecular and Crystal Structure of Dimethyl Sulfoxide, $(CH_3)_2SO$. *Acta Crystallogr.* **1966**, *21*, 12−20.
(70) Renault, E.; Le Questel, J.-V. Selenoxides Are Better Hydrogen-Bond Acceptors Than Sulfoxides: A Crystallographic Database and Theoretical Investigation. *J. Phys. Chem. A* **2004**, *108*, 7232−7240.
(71) Quack, M.; Willeke, M. Theory of Stereomutation Dynamics and Parity Violation in Hydrogen Thioperoxide Isotopomers $^{1,2,3}HSO^{1,2,3}H$. *Helv. Chim. Acta* **2003**, *86*, 1641−1652.
(72) Yurchenko, S. N.; Yachmenev, A.; Thiel, W.; Baum, O.; Giesen, T. F.; Melinkov, V. V.; Jensen, P. An Ab Initio Calculation of the Vibrational Energies and Transition Moments of HSOH. *J. Mol. Spectrosc.* **2009**, *257*, 57−65.
(73) Ovsyannikov, R. I.; Melnikov, V. V.; Thiel, W.; Jensen, P.; Baum, O.; Giesen, T. F.; Yurchenko, S. N. Theoretical Rotation−Torsion Energies of HSOH. *J. Chem. Phys.* **2008**, *129*, No. 154314.
(74) Pelz, G.; Yamada, K. M. T.; Winnewisser, G. Torsional Dependence of the Effective Rotational Constants of H_2O_2 and H_2S_2. *J. Mol. Spectrosc.* **1993**, *159*, 507−520.
(75) Goumri, A.; Rocha, J.-D. R.; Laakso, D.; Smith, C. E.; Marshall, P. Computational Studies of the Potential Energy Surface for O(1D)+H_2S: Characterization of Pathways Involving H_2SO, HOSH, and H_2OS. *J. Chem. Phys.* **1994**, *101*, 9405−9411.
(76) Wolfe, S.; Schlegel, H. B. On the Constitution of Dimethyl Sulfoxide. *Gazz. Chim. Ital.* **1990**, *120*, 285−290.
(77) Li, G.; Li, Q.-S.; Xie, Y.; Schaefer, H. F. F + $(H_2O)_2$ Reaction: The Second Water Removes the Barrier. *J. Phys. Chem. A* **2013**, *117*, 11979−11982.
(78) de Grotthuss, C. J. T. Sur la Décomposition de l'eau et des Corps Qu'elle Tient en Dissolution à l'aide de l'électricité Galvanique. *Ann. Chim. (Paris)* **1806**, *58*, 54−73.

DOI: 10.1021/acs.jpca.5b00779
J. Phys. Chem. A 2015, 119, 3500−3517

(79) Eigen, M. Proton Transfer, Acid–Base Catalysis, and Enzymatic Hydrolysis. Part 1: Elementary Processes. *Angew. Chem., Int. Ed. Engl.* **1964**, *3*, 1–19.
(80) Morachevskii, A. G. Theodor Grotthuss (to 220th Anniversary of His Birthday). *Russ. J. Appl. Chem.* **2005**, *78*, 166–168.
(81) Cukierman, S. Et tu Grotthuss. *Biochim. Biophys. Acta* **2006**, *1757*, 876–885.
(82) Marx, D. Proton Transfer 200 Years after von Grotthuss: Insights from Ab Initio Simulations. *ChemPhysChem* **2006**, *7*, 1848–1870.
(83) Markovitch, O.; Chen, H.; Izvekov, S.; Paesani, F.; Voth, A.; Agmon, N. Special Pair Dance and Partner Selection: Elementary Steps in Proton Transport in Liquid Water. *J. Phys. Chem. B* **2008**, *112*, 9456–9466.
(84) Mai, B. K.; Park, K.; Duong, M. P. R. T.; Kim, Y. Proton Transfer Dependence on Hydrogen-Bonding of Solvent to the Water Wire: A Theoretical Study. *J. Phys. Chem. B* **2013**, *117*, 307–315.
(85) Lanzotti, V. The Analysis of Onion and Garlic. *J. Chromatogr., A* **2006**, *1112*, 3–22.
(86) Block, E.; Dane, A. J.; Thomas, S.; Cody, R. B. Applications of Direct Analysis in Real Time Mass Spectrometry (DART-MS) in *Allium* Chemistry. 2-Propenesulfenic Acid and 2-Propenesulfinic Acids, Diallyl Trisulfane *S*-Oxide, and Other Reactive Sulfur Compounds from Crushed Garlic and Other Alliums. *J. Agric. Food Chem.* **2010**, *58*, 4617–4625.

DOI: 10.1021/acs.jpca.5b00779
J. Phys. Chem. A 2015, 119, 3500–3517